crystals

MDPI

Review

Potential of Recycled Silicon and Silicon-Based Thermoelectrics for Power Generation

Solco Samantha Faye Duran [1], Danwei Zhang [1], Wei Yang Samuel Lim [1], Jing Cao [1], Hongfei Liu [1], Qiang Zhu [1], Chee Kiang Ivan Tan [1], Jianwei Xu [1], Xian Jun Loh [1] and Ady Suwardi [1,2,*]

[1] Institute of Materials Research and Engineering, Agency for Science, Technology and Research, Singapore 138634, Singapore; solco_samantha_from.tp@imre.a-star.edu.sg (S.S.F.D.); zhang_danwei@imre.a-star.edu.sg (D.Z.); samuel_lim@imre.a-star.edu.sg (W.Y.S.L.); cao_jing@imre.a-star.edu.sg (J.C.); liuhf@imre.a-star.edu.sg (H.L.); zhuq@imre.a-star.edu.sg (Q.Z.); ivan_tan@imre.a-star.edu.sg (C.K.I.T.); jw-xu@imre.a-star.edu.sg (J.X.); lohxj@imre.a-star.edu.sg (X.J.L.)

[2] Department of Materials Science and Engineering, National University of Singapore, Singapore 117575, Singapore

* Correspondence: ady_suwardi@imre.a-star.edu.sg

Abstract: Thermoelectrics can convert waste heat to electricity and vice versa. The energy conversion efficiency depends on materials figure of merit, zT, and Carnot efficiency. Due to the higher Carnot efficiency at a higher temperature gradient, high-temperature thermoelectrics are attractive for waste heat recycling. Among high-temperature thermoelectrics, silicon-based compounds are attractive due to the confluence of light weight, high abundance, and low cost. Adding to their attractiveness is the generally defect-tolerant nature of thermoelectrics. This makes them a suitable target application for recycled silicon waste from electronic (e-waste) and solar cell waste. In this review, we summarize the usage of high-temperature thermoelectric generators (TEGs) in applications such as commercial aviation and space voyages. Special emphasis is placed on silicon-based compounds, which include some recent works on recycled silicon and their thermoelectric properties. Besides materials design, device designing considerations to further maximize the energy conversion efficiencies are also discussed. The insights derived from this review can be used to guide sustainable recycling of e-waste into thermoelectrics for power harvesting.

Keywords: silicon; waste silicon; semiconductor; energy harvesting; electronic waste; thermoelectrics; solar cell waste

Citation: Duran, S.S.F.; Zhang, D.; Lim, W.Y.S.; Cao, J.; Liu, H.; Zhu, Q.; Tan, C.K.I.; Xu, J.; Loh, X.J.; Suwardi, A. Potential of Recycled Silicon and Silicon-Based Thermoelectrics for Power Generation. *Crystals* **2022**, *12*, 307. https://doi.org/10.3390/cryst12030307

Academic Editor: M. Ajmal Khan

Received: 9 January 2022
Accepted: 18 February 2022
Published: 22 February 2022

1. Introduction

The increasing trend in energy generation worldwide is accelerating with a high of 162,194 TWh recorded in 2019, 21% more in comparison with a decade ago [1]. With this trend, it is imperative to explore various sources of energy, extending our options from finite natural resources and current methods of sustainable energy generation. Despite the development and advances in renewable energy sources, energy conversion is never completely efficient.

Energy generation, whether by fuel combustion or by conversion from other energy forms, usually involves a certain degree of heat loss to the environment. This heat loss becomes more pronounced at higher operating temperatures due to the large thermal difference between the source, the mechanical components, and the surroundings, promoting energy dissipation by radiation. Additionally, the waste heat produced, if not sufficiently dissipated, can be counterproductive to energy generation. For example, in a study conducted by Benghanem et al., it was shown that the efficiency of photovoltaic cells past the optimal operating temperature decreases by 0.5% with every °C increase [2]. It may then be expedient to focus on improving the energy conversion efficiencies in high-temperature applications whereby the residual heat prevents optimal performance to a larger extent.

In addition, attention should be directed to applications that not only incur the most heat loss but also utilize a large amount of fuel to further amplify economic benefits from a more efficient energy conversion. One example would be commercial aircraft, which are consuming up to 95 billion gallons of diesel in 2019 (before the coronavirus pandemic) due to the booming aviation industry, [3–10]. Furthermore, extra consideration should be taken for applications that utilize scarce material as energy sources, such as radioisotope thermoelectric generators (RTGs) powered by naturally occurring but limited radioactive oxides. To fully maximize the energy conversion processes in these applications, waste heat can be harvested and converted into electricity, which can be achieved through the use of thermoelectric generators (TEGs).

In this review, the conversion of energy from heat to electricity through thermoelectric materials will be explored in the context of high-temperature applications, such as commercial planes and deep space exploration. While a wide range of thermoelectric materials and devices have been studied up till now for low- and medium-temperature applications, such as utilizing body heat and waste heat from devices, this review will focus on applications requiring an operating temperature of >800 K. In addition, special emphasis will be placed on the potential of recycled materials, specifically silicon, for such application, keeping sustainability in mind. Furthermore, the thermoelectric materials commercially used in these applications will be analyzed in detail, focusing on their strengths and weaknesses as a thermoelectric material for high-temperature applications, common synthesis methods, doping, and modification for the optimization of their performance. Finally, device designing considerations will also be discussed to comment on the requirements of a suitable thermoelectric module in the context of the aforementioned high-temperature applications of commercial aviation and space voyages.

2. Thermoelectric Devices

The thermoelectric effect can be described as the interconversion of a thermal gradient and potential difference due to the migration of charges. The Seebeck effect, utilized in thermoelectric generators, occurs when there is a temperature difference across a suitable material. Charges travel from the heat source to the heat sink, causing one end of the material to be more negatively charged than the other. Subsequently, there will exist a potential difference between the hot side and the cold side, and when this material is connected in a circuit, a current will be generated, as illustrated in Figure 1.

The effectiveness of a thermoelectric material is measured by its dimensionless figure of merit (zT), which is calculated in Equation (1). The zT of a material is strongly linked to the efficiency of the thermoelectric device, which can be calculated using Equation (2) [11]. Maximizing zT has shown to be challenging due to the interconnectedness of its constituent factors. Additionally, the efficiency ceiling for any thermoelectric material is limited by the Carnot component $\frac{\Delta T}{T_c}$, which suggests that a larger temperature difference will reap better energy conversion efficiencies.

$$zT = \frac{S^2\sigma}{\kappa}T \tag{1}$$

$$\eta_{max} = \frac{\Delta T}{T_H}\frac{\sqrt{1+ZT_{avg}}-1}{\sqrt{1+ZT_{avg}}+\frac{T_c}{T_h}} \tag{2}$$

From a materials perspective, the performance of the thermoelectric can be altered using various methods due to the different components contributing to a single parameter. For instance, thermal conductivity comprises lattice (κ_{lat}), bipolar (κ_{bi}), and electrical (κ_{ele}) components [12–21]. Much of the work in decreasing thermal conductivity is aimed towards κ_{lat}, utilizing strategies such as downscaling and isovalent substitution, which hinder the transport of heat-carrying acoustic phonons [22–34]. More recently, machine learning has been popularly used in conjunction with materials science discovery and air materials development [35–38]. However, the effectiveness of these strategies is limited according to the defect type and the wavelengths of phonons [18,38–42]. Alternatively,

other strategies, such as band structure modulation, entropy engineering, and preferential scattering of minority carriers, can be explored, which aim to improve other components of thermal conductivity as well [43–53]. More recently, a fresh perspective on engineering next-generation high-performance thermoelectrics has been reported, which includes low doping, in contrast to the "golden range of carrier concentration" [54,55].

To date, the majority of high-performing thermoelectric materials are chalcogenides, such as SnSe-, GeTe-, PbTe-, PbSe-, and Bi_2Te_3-based materials [56–75]. In addition, efforts using both theoretical and experimental and even machine learning approaches are continued to be spent on discovering and improving materials performances [66,76–92]. However, despite these efforts, the underlying power conversion efficiency also depends on the application temperature. For instance, there has been relatively less focus on high-temperature thermoelectrics, presumably due to their low materials performance. However, this can be offset by the fact that at such high-temperature gradient, the overall power conversion efficiency will be decent, considering the relatively high Carnot efficiency.

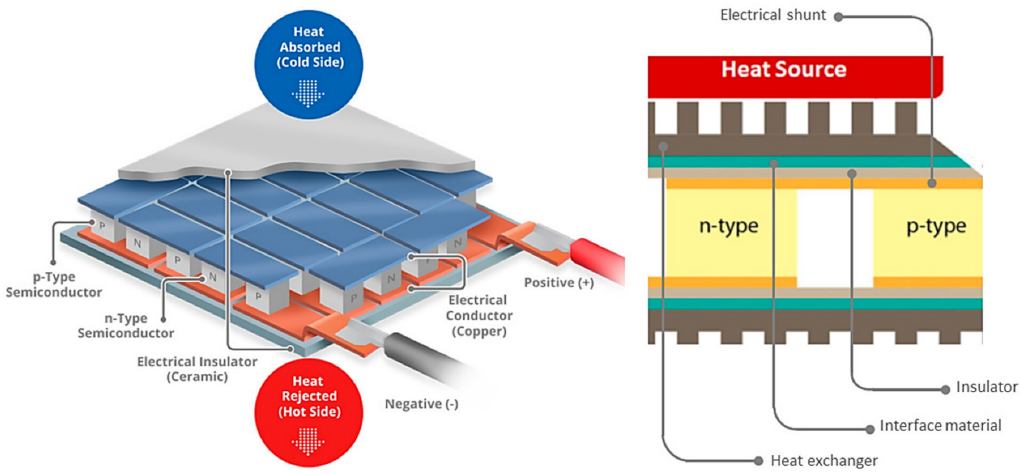

Figure 1. Basic configuration of a thermoelectric module and its working principle for TEG and TEC. (**a**) Schematic of heat transport from cold side to hot side when electric current is applied to thermoelectric cooler. (**b**) Cross-section of a typical thermoelectric module consisting of thermal and electrical insulation and interface materials. Reproduced with permission from [93].

For device applications, there are multiple factors to consider. First, the properties of the p-type and n-type legs should be comparable to maximize the device zT and optimize the efficiency of the module. The requirements for properties matching between p-type and n-type legs can be categorized into:

2.1. Geometrical Matching

This involves tailoring the dimension of the respective leg according to the intrinsic properties. This is done to ensure a similar level of heat current density and electrical current density passing through both legs. Based on the electronic and thermal transport data, the ideal form factors for the device should be as close as possible to the following values:

$$\frac{L_n A_P}{L_p A_n} = \left(\frac{\rho_p \kappa_n}{\rho_n \kappa_p}\right)^{1/2} \tag{3}$$

where ρ and κ represent the electrical resistivity and thermal conductivity of both p-type and n-type legs.

2.2. Compatibility Factor Matching

This is a less intuitive requirement. It was popularized by Snyder et al. in the early 2000s [94]. Compatibility factor is important to ensure that not only both p-type and n-type legs have the same heat or electrical current density, but also the relative current density is similar in both legs. The concept of relative current density is defined as:

$$u = \frac{J}{k\Delta T} \tag{4}$$

where u is the relative current density, J is the electrical current density, and $\kappa\Delta T$ is the thermal heat flux through the thermoelectric leg. At a particular temperature, the value of u, which maximizes the overall efficiency, is defined as s (compatibility factor):

$$s = \frac{\sqrt{1+zT}-1}{ST} \tag{5}$$

where s, zT, and S represent compatibility factor, figure of merit, and Seebeck coefficient, respectively. Intuitively, for materials with high Seebeck coefficient (and generally low electrical conductivity), only low electrical current for a given heat flux is allowed to pass through the material to maximize its efficiency by minimizing loss due to Joule heating.

In addition to electrical and thermal matching, both thermoelectric legs need to have similar coefficients of thermal expansion [95]. As the device will be subjected to a temperature gradient and the materials expand with heating, it is important to ensure that all legs expand and contract with minimal differences as it can introduce strain to the points of connection, causing the legs to detach from the interconnects and breaking the circuit. Another consideration would be the choice of insulating layer used to fill the space between the thermoelectric legs. A suitable insulator is important to reduce the heat transfer from the heat source to the heat sink to preserve the temperature gradient and maximize the power output of the device. Additional requirements are considered based on the specific application in which the thermoelectric module is used as environmental factors can also affect the modifications required for the device. Some examples of external factors are high pressure, high operating temperature, vibrational stress, humidity, geometry of the surface for application, extremely low temperatures that can cause icing, and the required duration of service. Some of these will be addressed at a later section of the review regarding the conditions on commercial aircraft and space voyages.

Notwithstanding, the fabrication of a highly efficient thermoelectric module is first dependent on the performance of the individual thermoelectric leg. It is important to compare the efficiency of thermoelectric materials based on their operating temperatures. Materials with wide band gaps are most suitable for high-temperature applications as bipolar conduction can be avoided. Through modifications, the peak figure of merit for each material may be improved. However, another avenue to explore is achieving modest zT for a wider range of temperatures to broaden the scope of applications for a single material (i.e., high average zT over the operating temperature range). Until an effective solution can be realized to widen the operating temperature of the best-performing materials, it is prudent to focus efforts on deploying the currently available TEGs into applications where there is potential to reap large benefits, such as in high-temperature applications.

3. Thermoelectric Applications

3.1. In Commercial Airplanes

In terms of applications, a thermoelectric module for power generation can potentially be used for applications where a high hot source temperature is present, such as automobiles or aircraft. Crane et al. reported the integration of TEG into the exhaust line of BMW X6 and Lincoln MKT [96]. It was found that power up to 500 W was achieved during operation after a steady state was reached. This was achieved at an engine operation of 3000 RPM,

105 Nm, and a coolant temperature of 30 °C with a flow rate of 20 liters per minute. A schematic of the parts and assembly is shown in Figure 2.

Besides automobiles, commercial airplanes can be a large source of thermal energy at multiple stages of their operation. The copious amount heat generated by the engines, coupled with the low temperatures at high altitudes, presents a large temperature gradient and an opportune situation to exploit waste heat harvesting using TEGs. The air surrounding the mechanical and electrical components of aircraft is heated to various extents according to the mode of operation. According to a 2002 report by the National Academy of Sciences (Washington, DC, USA), the air at the engine bleed was measured to be 170 °C for ground operations and 350 °C at take-off, which is when the maximum power is utilized [97]. Considering the heat loss due to radiation, should a thermoelectric be implemented, the actual temperature of the surface in direct contact with the aircraft components can be expected to be higher than the reported values.

The use of thermoelectric devices can provide further environmental benefits and profit the aviation industry as well. First, by converting waste heat into electricity, the carbon emissions of aircraft would be reduced. Globally, in 2019, humans produced over 43 billion tonnes of CO_2, 12% of which was contributed by transport sources and commercial aircraft, taking up 2% of the total CO_2 production. Summarizing the contributions of aircraft worldwide, 915 million tonnes of CO_2 was produced in 2019 alone [98]. Although the impact on climate change from the cumulative use of automobiles and the production of electricity surpasses that of commercial aviation, passenger air travel is producing the fastest growth of individual emissions, despite a significant improvement in the efficiency of aircraft operations over the last 60 years [99]. Following this trend, it can be forecasted that the aviation industry will continue to grow in the coming years and possibly contribute a larger share to the CO_2 production worldwide. Therefore, it is worthwhile to invest in targeting the reduction of emissions from the commercial aviation industry.

Moreover, according to a 2009 report by Boeing Research and Technology, harvesting waste heat can reduce fuel consumption of aircraft by up to 0.5%, which is equivalent to a savings of USD 12.075 M in monthly operations [100]. Excluding these major benefits of utilizing thermoelectric devices for commercial aircraft, additional gains include potential weight reduction when thermoelectric coolers replace traditional coolants and improve system efficiencies of other auxiliary systems used in planes, which tend to overheat with long operating hours. Additionally, thermoelectric coolers have no mechanical parts, which minimizes the amount of maintenance required.

Thermoelectric applications in aircraft have taken a backseat with the harvested energy used to power auxiliary operations. One popular application is the powering of wireless sensor networks (WSNs) [101]. WSNs monitor the state of the physical environment at the area of deployment and communicate the status to a central location for data collection or analysis. This is used to minimize redundant electrical connections in the already-complex wiring system in the aircraft. These sensor nodes are utilized for wireless avionics intracommunications (WAIC), and the exchange of data between different components in the same aircraft can be programmed to elicit a desired response for specific conditions. For example, when the cabin is detected to have low oxygen levels by the WSNs, the information can be broadcasted to the other nodes to discharge oxygen masks from above the passenger seats [102].

Additionally, WSNs are commonly used for the structural health management (SHM) of buildings, and its potential use in aircraft has been recognized as well [104,105]. SHM utilizes the information gathered by WSNs to signal for symptoms of deterioration. For instance, nodes can be used for comparative vacuum monitoring and are installed in areas more prone to fatigue. Initially, the area is maintained in vacuum conditions by sealing interfaces using adhesives. When mechanical motion causes cracks in the components, air will be able to escape and break the initially induced vacuum. The change in pressure will be registered by the sensor node, and the maintenance team can be alerted for repair. This moves the health management of structures to condition-based maintenance

instead of scheduled maintenance and, hence, enhances the reliability and safety of the aircraft as symptoms of component damage can be detected and remedied faster, avoiding catastrophic failure [106].

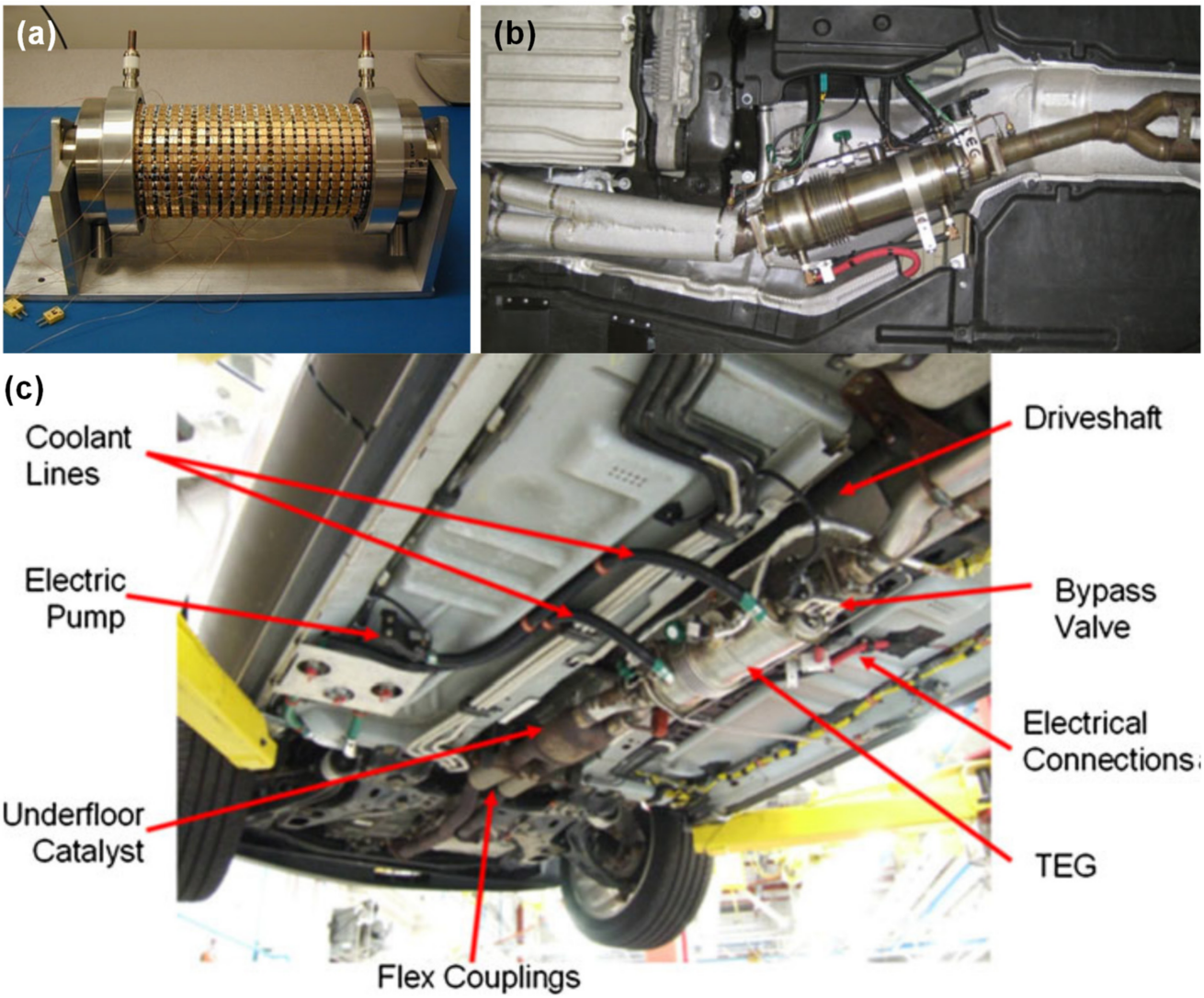

Figure 2. (**a**) Bi_2Te_3-based cylindrical TEG device. (**b**) TEG integration into the exhaust line of the BMW X6 prototype vehicle. (**c**) Integration of the TEG into the underfloor of the test vehicle. Figure reproduced with permission from [96,103].

Taking inspiration from TEGs implemented in automobiles, the device design for aircraft application can be modelled similarly. In terms of location, the aircraft fuselage has been a popular choice for study in the past. Simulations have shown that the energy generated averages 3.3 V with power management systems, sufficient to sustain WSNs [107]. As the fuselage does not have significant curvature, prototypes developed tend to use flat TEGs, which was also seen in a study by Elefsiniotis et al. [108].

Other alternative locations worth exploring include the aircraft engine and nozzle, where a large amount of heat is expended throughout the course of the flight [109]. However, as the geometry at these areas is slightly more complicated than that of a flat surface, more considerations are included in designing the device. For example, due to the curvature of the aircraft nozzle, it may be more practical to consider annular TEGs whereby the width of the thermoelectric legs is nonuniform to allow for the device to wrap around the surface. A study conducted by Shen et al. concluded that the use of ATEGs for curved surfaces reduces contact resistance compared with the flat version [110]. Ultimately, this

could possibly improve the TEG performance and energy harvesting efficiency of the system. Hence, for each location that we intend to apply TEG, the geometry, among other factors, should be taken into consideration.

3.2. In Spacecraft

The use of thermoelectric materials in space voyages is a niche application, highlighting the suitability of the energy generation method unparalleled by other sustainable forms. They are the key component of radioisotope thermoelectric generators (RTGs), which supply power to satellites, space probes, and unmanned remote facilities. An RTG is a form of nuclear battery that employs the Seebeck effect to harvest the heat generated by the decay of radioactive material. Figure 3 shows the schematic multimission radioisotope thermoelectric generator (MMRTG) [111]. GPHS (general purpose heat source) Pu238 heat source modules were used to fuel the system, with an 87.5 year half-life. This is surrounded by the thermoelectric modules. The other side of the thermoelectric modules is retained at a lower temperature as heat is dissipated by the radiator fins. This mode of energy generation is most useful for space voyages as other forms of energy generation can be costly or unreliable or have a large weight penalty.

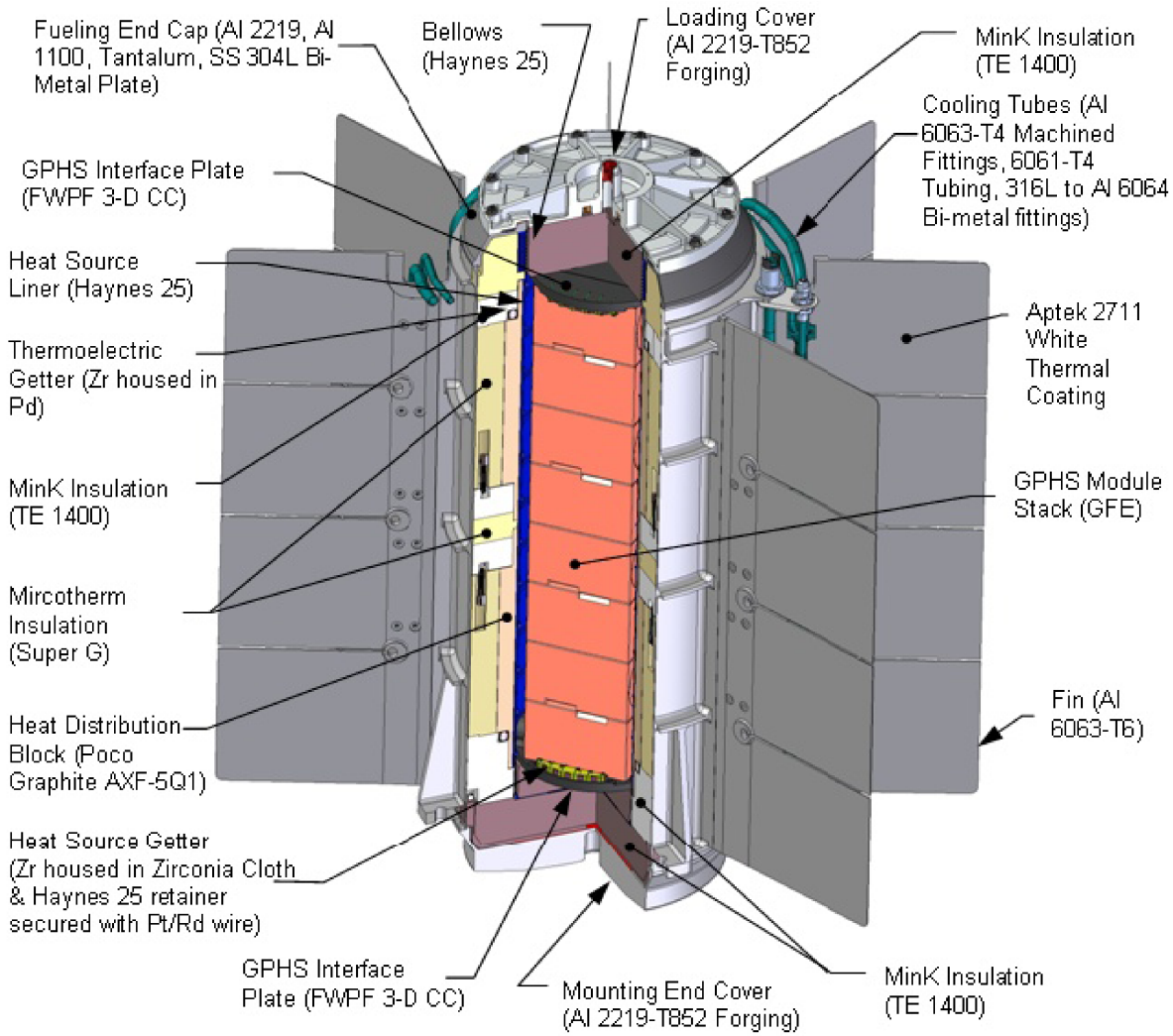

Figure 3. Schematic illustration of a multimission radioisotope thermoelectric generator (MMRTG). Figure extracted from open source (https://commons.wikimedia.org/wiki/File:MMRTG_schematic_-_english_labels.png; accessed on 18 January 2022).

Thermoelectrics are generally used for space applications because although photovoltaics have higher energy conversion efficiency, they will be an inefficient mode of energy generation as the rotation of the planets limits the amount of light that can be harvested, especially for voyages farther from the sun. The employment of hydropower or wind energy generation is also dependent on our current understanding of the environment in space. In the case of satellites that are launched to orbit in vacuum, these modes of energy generation would be unsuitable. Additionally, a large number of batteries or fuel cells would be required to power the mission in the entirety of its duration.

An important consideration is the ease of maintenance or replacement of the energy source. It would be inconvenient to consistently send manpower into space to replace or repair the power source. Hence, it is intuitive to gravitate towards RTGs as thermoelectric-based generators have a high power-to-mass ratio, require minimal maintenance due to the absence of mechanical components, and are self-sustaining in the presence of a temperature difference, which allows the user to customize the power source to the power and duration required [112]. To date, the total initial power generation capabilities for space voyages is on a climbing trend from 2.7 W for Transit 4A, which was launched in 1961, to 113 W for the recent Mars Curiosity rover. This can be partly attributed to advances in RTG technologies over the years [113]. The difference between the technologies is further detailed by NASA in Table 1 [114]. It can be observed that different RTG technologies are utilized depending on the external conditions, such as the atmosphere and the operating temperature of the RTG. Consequently, different thermoelectric materials may be used to fulfill the different requirements to maximize the efficiency of the RTG. From the table, it is evident that RTG technology has evolved significantly over the years and is versatile for missions of various durations and in different environments.

Table 1. Types of RTG technologies by NASA. Reproduced with permission from "NASA Special Session: Next-Generation Radioisotope Thermoelectric Generator (RTG) Discussion" from the National Aeronautics and Space Administration, 2017 [114].

Acronym	Definition	Descriptions	Power/GPHS	T_h (K)
GPHS-RTG	General-purpose heat source RTG	This RTG was designed to operate in vacuum only. It was flown on PNH, Cassini, and other missions. Not a modular system.	290/10	1273
MMRTG	Multimission RTG	Operated in vacuum and atmosphere. Flown on the Curiosity rover. Not a modular system.	110/8	803
eMMRTG	Enhanced multimission RTG	A potential enhanced version of the MMRTG. Designed to operate in vacuum and atmosphere. Not a modular system. While not yet approved for development, it is extremely well modelled, and its system requirements are well understood.	145/8	873

While the usage of RTGs has proven successful over the decades and further development is ongoing, the conversion efficiencies of the thermoelectric modules can still be further improved. Increasing the efficiency of the thermoelectric could suggest that the same missions can be launched using less radioisotopes for the heat source. This is pertinent for the continuation of space voyages as the currently most used radioisotope, ^{238}Pu, is scarce [115]. Hence, it is financially and environmentally beneficial to study possible avenues of improvement in the thermoelectric materials used for RTGs.

One strategy for maximizing the power harvested by RTGs is the use of segmented thermoelectric legs. This strategy utilizes a combination of thermoelectric materials for different operating temperatures and will be further explained in a later section. Table 2 shows the different thermoelectric materials used for low-, mid-, and high-operating temperatures utilized by NASA so far in their space voyages. Both commercial aircraft and RTGs emit large amounts of heat energy, which, when harvested, can be channeled and converted to electrical energy and improve the efficiency of the applications.

Table 2. p-Type and n-type thermoelectrics used for low, mid, and high temperatures. Reproduced with permission from "NASA Special Session: Next-Generation Radioisotope Thermoelectric Generator (RTG) Discussion" from the National Aeronautics and Space Administration, 2017 [114].

Operating Temperature	*n-Type*			*p-Type*		
	Low	**Mid**	**High**	**Low**	**Mid**	**High**
1	$Bi_2Te_{3-x}Se_x$	1-2-2 Zintl	$La_{3-x}Te_4$ composite	$Bi_{2-x}Sb_xTe_3$	9-4-9 Zintl	14-1-11 Zintl
2	$Bi_2Te_{3-x}Se_x$	1-2-2 Zintl	$La_{3-x}Te_4$	$Bi_{2-x}Sb_xTe_3$	9-4-9 Zintl	14-1-11 Zintl
3	$Bi_2Te_{3-x}Se_x$	SKD	$La_{3-x}Te_4$ composite	$Bi_{2-x}Sb_xTe_3$	SKD	14-1-11 Zintl
4	$Bi_2Te_{3-x}Se_x$	SKD	$La_{3-x}Te_4$	$Bi_{2-x}Sb_xTe_3$	SKD	14-1-11 Zintl
5	$Bi_2Te_{3-x}Se_x$	$Mg_2Si_{1-x}Sn_x$	$La_{3-x}Te_4$ composite	$Bi_{2-x}Sb_xTe_3$	Tetrahedrite	14-1-11 Zintl
6	$Bi_2Te_{3-x}Se_x$	n-HH	$La_{3-x}Te_4$ composite	$Bi_{2-x}Sb_xTe_3$	p-HH	14-1-11 Zintl
7	$Bi_2Te_{3-x}Se_x$	PbTe	$La_{3-x}Te_4$ composite	$Bi_{2-x}Sb_xTe_3$	TAGS	14-1-11 Zintl
8	$Bi_2Te_{3-x}Se_x$	Nano PbTe	$La_{3-x}Te_4$ composite	$Bi_{2-x}Sb_xTe_3$	TAGS	14-1-11 Zintl
9	-	$Mg_2Si_{1-x}Sn_x$	Nano SiGe	-	$MnSi_{1.7}$	Nano SiGe
10	-	-	$La_{3-x}Te_4$ composite	-	-	14-1-11 Zintl
11	-	-	$La_{3-x}Te_4$	-	-	-
12	-	-	Nanobulk SiGe	-	-	Nanobulk SiGe
13	$Bi_2Te_{3-x}Se_x$	-		$Bi_{2-x}Sb_xTe_3$	-	
14	$Bi_2Te_{3-x}Se_x$	-	$La_{3-x}Te_4$ composite	$Bi_{2-x}Sb_xTe_3$	-	14-1-11 Zintl
15	$Bi_2Te_{3-x}Se_x$	SKD	-	$Bi_{2-x}Sb_xTe_3$	SKD	-
16	$Bi_2Te_{3-x}Se_x$	PbTe	-	$Bi_{2-x}Sb_xTe_3$	TAGS	-
17	$Bi_2Te_{3-x}Se_x$	$Mg_2Si_{1-x}Sn_x$	$La_{3-x}Te_4$	$Bi_{2-x}Sb_xTe_3$	Tetrahedrite	14-1-11 Zintl
18	$Bi_2Te_{3-x}Se_x$	n-HH	$La_{3-x}Te_4$	$Bi_{2-x}Sb_xTe_3$	p-HH	14-1-11 Zintl
19	$Bi_2Te_{3-x}Se_x$	PbTe	$La_{3-x}Te_4$	$Bi_{2-x}Sb_xTe_3$	TAGS	14-1-11 Zintl
20	$Bi_2Te_{3-x}Se_x$	nano PbTe	$La_{3-x}Te_4$	$Bi_{2-x}Sb_xTe_3$		14-1-11 Zintl
21	-	-	$La_{3-x}Te_4$	-	-	14-1-11 Zintl

4. Materials Selection

4.1. Silicon

Silicon is the second most earth-abundant element in the earth's crust, and the most abundant element used in modern-day technologies [116]. Its popularity partially stems from the nontoxic and relatively unreactive nature of derivatives, such as silica and silicates, at room temperature [117]. Consequently, the sheer volume of silicon being used has accelerated the rate of production of waste materials. Mainstream applications, such as electronics and semiconductors, typically require ultrapure silicon, which undergo a tedious and expensive purification process. Thermoelectric applications are also affected by defects, albeit less sensitively compared with other applications, which suggests that the cost of fabrication can be much cheaper. Intrinsically, bulk silicon has a high thermal conductivity of ~150 Wm^{-1} K^{-1} at room temperature. Fortunately, such parameters can be optimized to give a decent zT value. Several works in the recent two decades have studied the potential of elemental silicon as a thermoelectric material in various forms [118–123]. For instance, a work conducted by Bux et al. compared the performances of synthesized nanostructured bulk Si and $Si_{0.8}Ge_{0.2}$ and found that the thermal conductivity of nanostructured bulk Si could be significantly reduced and ultimately produce a zT of 0.7 at 1200 K. While in the initial days, extensive silicon purification did not pose much of a problem, the waste from the first-generation electronics boom in recent years has caused it to become a major issue. This problem is exacerbated by the exponential increase in solar cell waste [124]. For instance, it is often economically and technologically not feasible to recycle used

silicon (often alloyed or doped with other elements) for delicate use, such as in the high-performance electronics industry. In addition, the process of cutting Si ingots with wire for solar cell fabrication leads to a material loss of 40% in the form of kerf [125]. Fortunately, this is where thermoelectrics can play a vital role. As a majority carrier device (as opposed to a minority carrier device, such as photovoltaics), thermoelectrics are generally less defect sensitive, and existing impurities may even be beneficial to their performance instead. Additionally, since silicon is safe to handle in comparison with other compounds composed of toxic or harmful elements, such as Pb or Te, the mass production of silicon-based thermoelectrics would not pose any concerns to human or environmental health.

4.2. Recycled Silicon

High-performance thermoelectrics can often be achieved via defect engineering, where lattice defects or impurities are deliberately introduced into the materials to improve their electrical or thermal properties. This makes thermoelectrics a perfect target for recycling (or upcycling) silicon-based electronics waste (e-waste) and other technological silicon waste. Figure 4 shows a schematic of how thermoelectrics can benefit from the existing defects of the waste material.

Figure 4. Schematic showing waste upcycling of industrial and agricultural waste into thermoelectrics. Figure from Bahrami et al. [125]. Copyright 2020, Wiley (Weinheim, Germany).

Recycling waste material into thermoelectrics is an area that has been explored for other elements, such as bismuth [126,127]. Cai et al. recently explored the recyclability

of bismuth antimony telluride thermoelectrics and discovered that the combination of reprocessed $(Bi,Sb)_2Te_3$ scraps and nano-SiC showcased a better zT of 1.07 at 325 K even in comparison with the commercial alloy, which was 0.95. Further work conducted on the specifics of the nanocomposition yielded an improved zT of 1.33.

Similarly, the merits of upcycled silicon-based thermoelectrics has been recognized but not yet popularized, which undermines its potential in championing sustainable energy harvesting and cooling technologies. For instance, the pioneering encounter with recycled silicon thermoelectric stemmed from rice husks. Si-based compounds obtained from the valorization of rice husks were used by Bose et al. to synthesize Mg_2Si [128]. However, the results then were not particularly promising with a zT of 1×10^{-4} due to the impurities that were retained in the synthesis of the compound [129]. More recently, Ran et al. discovered that upcycled silicon from sawing waste, doped with phosphorous, achieved a power factor of 32 $\mu W\ cm^{-1}\ K^{-2}$ at 1273 K and, subsequently, a peak zT of 0.33 [130]. Comparatively, SiGe alloys (to be discussed later) performed with peak zT values reaching ~0.65 and ~1 in p- and n-type $Si_{80}Ge_{20}$, respectively, were consistently reported in multiple studies for temperatures of 900–950 °C.

Additionally, there is an abundance of silicon-based waste products as a result of the escalating rate of production of PV modules. Fabrication of such electronics produces by-products, such as SiC, diamond particles, metals, and oxidized silicon. While it may be intuitive to prioritize recycling precious and expensive materials, such as silver and gold, thankfully, in recent years, there has been more effort to recycle Si particles [131]. Aside from utilizing Si kerf for TE synthesis, other Si-based by-products can be purified and utilized for the synthesis of compounds, such as Mg_2Si. Isoda et al. [132] and Mesaritis et al. [133] successfully utilized Si kerf as a precursor to $Mg_2(Si,Ge,Sn)$ alloys, which perform competitively for TE made from commercial silicon.

It is worth noting that although recycled silicon does not have very high average figure of merit, the wide temperature gradient made available by the high operating temperature allows for a better Carnot efficiency, resulting in decent power conversion efficiencies. Figure 5a,b shows the power factor and figure of merit of silicon thermoelectrics processed from sawing waste from recent works. Although such number is nowhere near the recorded zT of thermoelectrics, it can still provide 5–7% power conversion efficiency based on Equation (2). Further optimization of the doping for recycled silicon can present opportunities for thermoelectrics with performances competitive with popular SiGe.

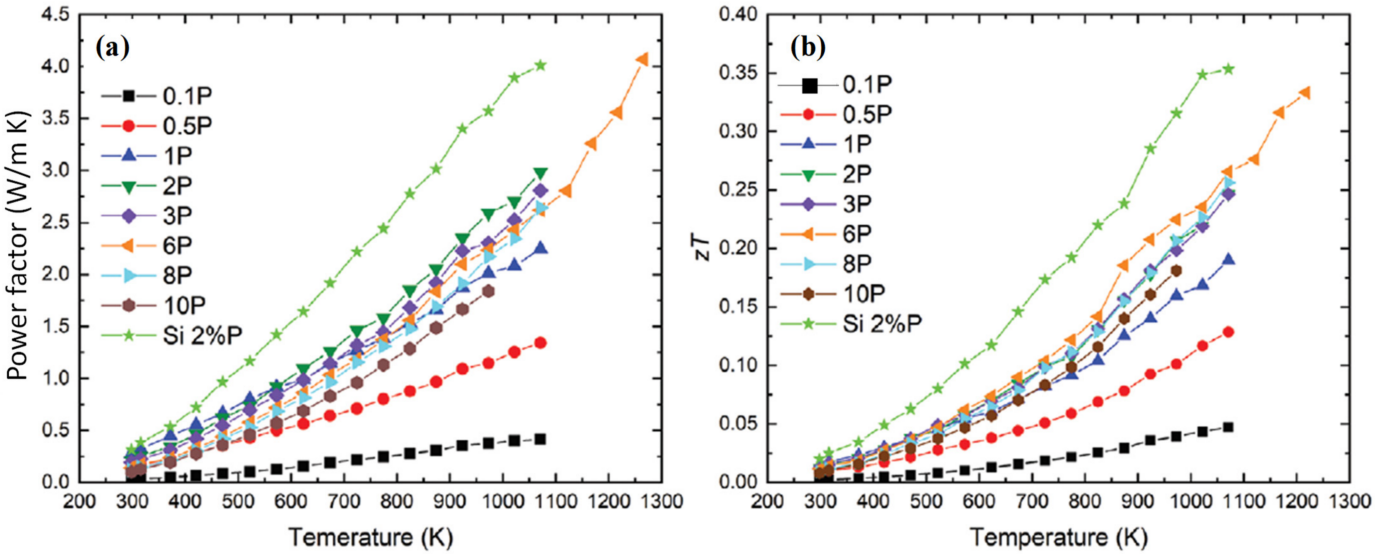

Figure 5. (**a**) Power factor and (**b**) figure of merit zT for silicon from sawing waste, with different levels of P doping. Figure from Ran et al. [130].

4.3. Silicon Germanium

Silicon germanium is a semiconducting alloy with a diamond crystal structure popularly used for high-temperature thermoelectric applications. The alloy is miscible at all ratios of SiGe but presents a challenge in consistent synthesis due to its complex phase diagram. Prior to the development of SiGe as a thermoelectric, silicon was the staple for high-temperature applications due to its abundance and nontoxicity. However, it is disadvantaged as a thermoelectric material due to its low electrical conductivity and high thermal conductivity. The conductivity of silicon can be improved through aliovalent doping of boron and phosphorus to create p-type and n-type semiconductors, respectively. However, this is insufficient to boost its performance as a thermoelectric without improvements in its thermal conductivity.

Conversely, germanium is also a semiconducting material with a small band gap of 0.66 eV. It exhibits good electrical conductivity and low thermal conductivity, making it a promising thermoelectric option for low-temperature applications. However, germanium is much less abundant than silicon at 1.5 parts per million and is also rather costly [134]. Hence, it is more frequently used as an alloying component to other thermoelectric materials, such as SiGe and GeTe.

The addition of Ge to a Si matrix introduces mass fluctuations, varying the lattice parameters as well. Dismukes modelled the relation between the lattice constant and the percentage Ge in 1964, slightly modifying Vegard's law, as shown in Equation (6) [135,136].

$$Si_{1-x}Ge_x(A) = 5.432 + 0.20x + 0.027x^2(A) \quad (6)$$

The mass fluctuations created due to the difference in atomic size of silicon and germanium scatters short-wave acoustic phonons, which contribute largely to the material's thermal conductivity. A paper by Virginia Semiconductor compares the electronic characteristics of Si, Ge, and some compositions of SiGe [137]. The electrical properties of the $Si_{1-x}Ge_x$ alloys vary proportionately to the amount of germanium added to the silicon matrix, reducing the resistivity and thermal conductivity while increasing the drift mobility of charge carriers.

The ratio of Si to Ge was studied for optimal composition to maximize the scattering of acoustic phonons, and it was found that a 20% substitution of Ge exhibited a significant decrease in thermal conductivity to ~9 W cm^{-1} K, and a further addition of Ge contributed insignificantly [138]. Additionally, Ge is about 100 times more costly as compared with Si [139]. Therefore, minimizing the required amount for substitution would be financially beneficial. The alloying of silicon and germanium in different ratios allows for the fabrication of thermoelectric materials with various operating temperatures due to the changes in the band gap. This offers a solution to silicon's shortcoming as a thermoelectric, presenting us with SiGe as an option for thermoelectric materials at high-temperature applications.

Adding on the promise of intrinsic SiGe, multiple modifications have been studied to further enhance the performance of this alloy, including nanostructuring, modulation doping, and various methods of synthesis. SiGe exhibits a complex phase diagram, as illustrated in Figure 6. There is a large separation between the solidus and liquidus lines, suggesting that the composition of the SiGe alloy is sensitive to temperature and the amount of Ge added.

According to a recent review by Basu et al., the solid-state synthesis of SiGe through mechanical alloying, followed by densification by hot pressing or spark plasma sintering, is the key to consistent replication of desired stoichiometry. Mechanical alloying is also a simple and economical method to produce homogeneous alloys with consistent grain sizes. Hot isostatic pressing utilizes a combination of temperature and pressure to densify the ball-milled powder. The alternative to hot pressing is spark plasma sintering (SPS), whereby a high current is applied through the sample, heating the sample while under compression. In comparison with SPS, hot pressing is less favored as it encourages grain

growth. Similar to silicon, p-type SiGe is most commonly synthesized by doping with boron and n-type with phosphorus.

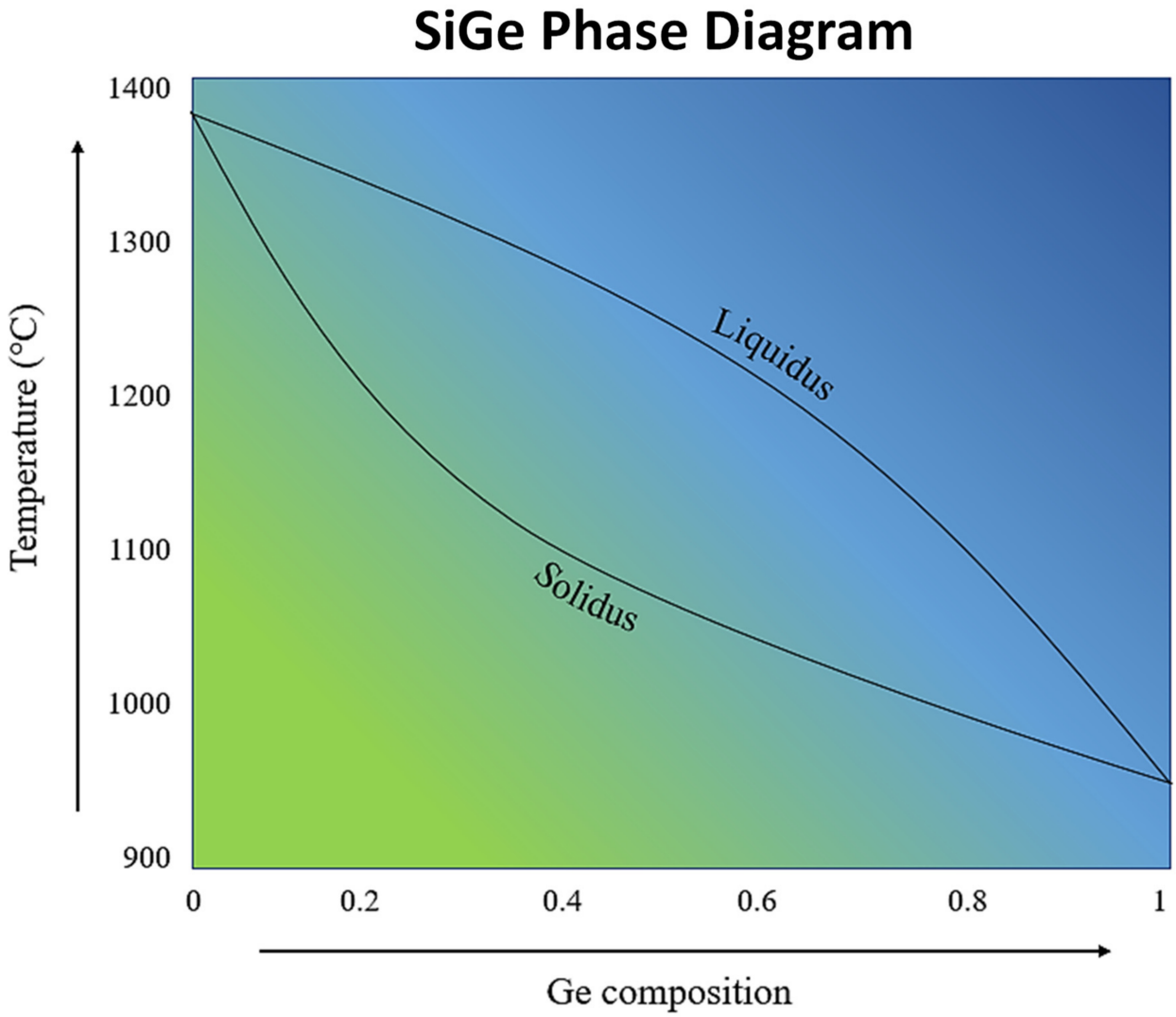

Figure 6. Phase diagram of SiGe. Figure reproduced with permission from "Towards a Fully Functional Integrated Photonic–Electronic Platform via a Single SiGe Growth Step" from Littlejohns et al., 2016 [140].

A popular strategy for enhancing the thermoelectric performance is modulation doping. Compared with uniform doping, modulation doping is the selective addition of dopants in spatially segregated areas, as shown in Figure 7. The clustered-doping method promotes higher charge mobility as the ionized dopants will be segmented into the designated areas and limit the electrostatic scattering of charges [141]. Hence, it can be expected that modulation doping will improve the power factor. However, it is also important to consider that the dopants have their own thermal conductivity. The higher thermal conductivity of the introduced precipitates limits the improvement of zT by the increase in power factor.

For example, a previous work conducted by Yu et al. demonstrated their three-dimensional modulation doping approach using a two-phase nanocomposite of different types of nanograins. In their study, an improvement of 40% was realized in the power factor of $Si_{80}Ge_{20}$ doped to 30% with $Si_{100}B$, forming the composite $(Si_{80}Ge_{20})_{0.7}(Si_{100}B_5)_{0.3}$ in comparison with $Si_{86}Ge_{14}B_{1.5}$. Conversely, for the n-type $Si_{84}Ge_{16}P_{0.6}$, the modulation-doped composite $(Si_{80}Ge_{20})_{0.8}(Si_{100}P_3)_{0.2}$ exhibited an improvement in power factor by 20%.

Despite the increase in power factor for both samples, the zTs did not improve due to the high thermal conductivity of the Si nanoparticles. Yu elaborated that the use of modulation doping strategies will inevitably bring about an increase in the electronic component as charge carriers are thermal carriers and also an increase in the lattice component when the nanoparticles have a higher thermal conductivity [143]. In turn, more attention should be directed to the reduction of the lattice component. This further modification was also discussed in his work.

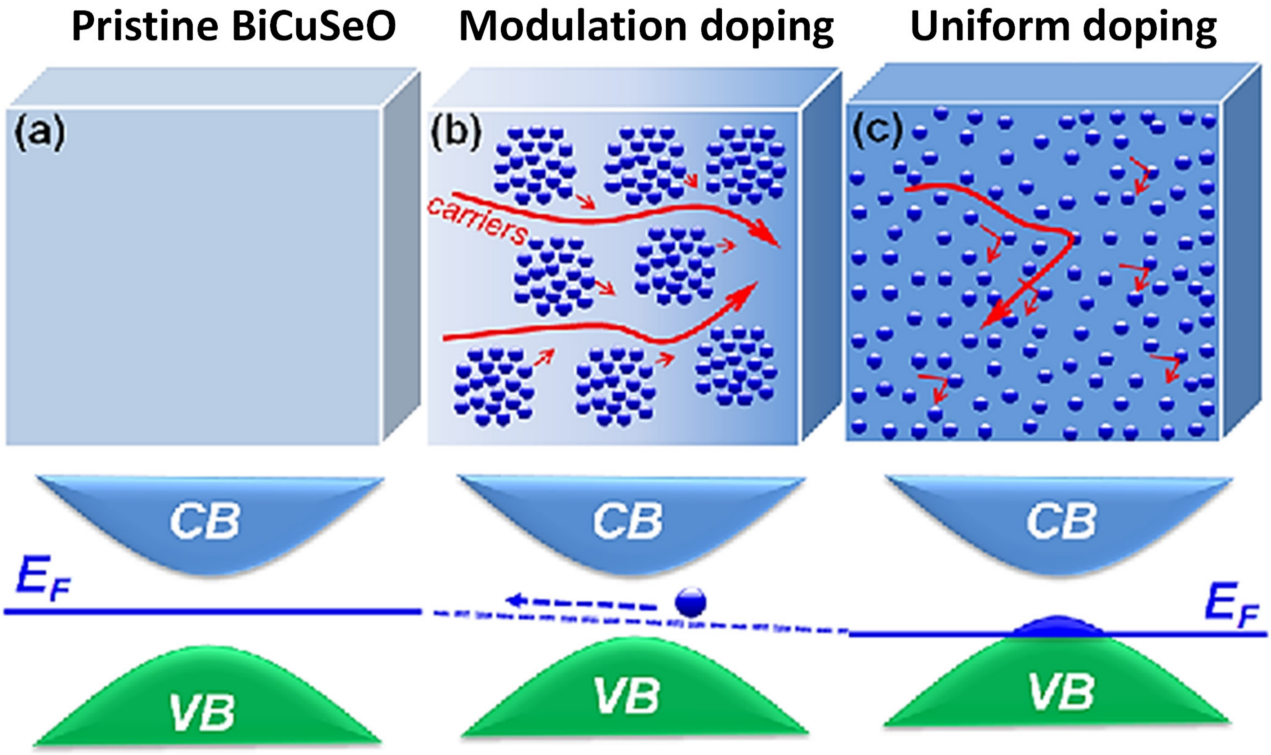

Figure 7. Schematic showing a carrier transport in (**a**) pristine BiCuSeO, (**b**) modulation-doped and (**c**) uniformly doped samples. Figure reproduced with permission from "High Thermoelectric Performance Realized in a BiCuSeO System by Improving Carrier Mobility through 3D Modulation Doping" from Pei et al., 2014 [142].

4.4. Other Silicon-Based Compounds

Aside from SiGe, many other Si-based compounds have been of interest for thermoelectric use due to silicon's crust abundance and nontoxicity. Each of these has its own merits and shortcomings, which will be briefly discussed in this section. To date, the compounds that have gained traction in the thermoelectric field are metal silicides, more specifically for alkali, alkaline, and transition metals. However, the optimal operating temperatures for each of them vary according to the alloying composition.

Ru_2Si_3 was once considered a potentially competitive high-temperature thermoelectric material, alongside SiGe alloys. Its interesting band structure suggested an initial extrapolated zT 50–300% higher than that of SiGe, assuming that the carrier mobility of Ru_2Si_3 trends similarly to that of silicon [144,145]. Sawade et al. synthesized undoped Ru_2Si_3, which boasted a zT of 0.32 at 900 K [146]. Despite further work on the compound, such as Mn doping, breakthroughs since then have been limited due to a lack of suitable dopants and scarcity concerns of elemental Ru [147].

Most other metal silicides are observed to be suitable for medium temperature applications. There is a wide array of transition metal silicides that have been developed for thermoelectric use, such as $MnSi_x$, $CrSi_2$, WSi_2, and $MoSi_2$. Within this category, good thermoelectric performance was exhibited by the higher manganese silicide (HMS) compounds, which exhibited a zT of 0.5–0.7 at 500 °C [148].

The superior performance of HMS partly stems from MnSi, which introduces energy barriers and improves carrier charge transport. In addition, HMS alloys are mechanically robust and highly resistant to oxidation, making their fabrication into module easier. Many studies have been conducted to further improve the performance of HMS, such as nanostructuring, Ge substitution, Al substitution, and nanoinclusions, with some degree of success. However, more studies could be conducted in improving the power factor of HMS to further boost zT.

Likewise, recycled silicon has been studied for the synthesis of Mg_2Si. Akasaka et al. and Honda et al. achieved a zT of 0.5–0.6 at 800–860 K, and Isoda et al. and Mesaritis et al. synthesized Mg_2(Si,Ge,Sn) thermoelectrics with purified Si kerf and reported a decent zT. The values achieved are competitive with pristinely synthesized thermoelectrics, and this opens up an opportunity for cheaper and more sustainable materials.

Si-based materials have exhibited great potential in waste heat harvesting at medium to high temperatures. The choice of material for TE module fabrication and subsequently deployment in commercial aviation or aerospace application warrants additional consideration of other aspects of the material to ensure that the device performs with optimal power efficiency for a reasonable lifetime.

5. Consideration for High-Temperature Devices

5.1. Device Design

Developing unicouples for a functional device, especially for applications that concern human safety or high cost, needs to account for multiple considerations. This is partly the reason more attention should be directed to developing thermoelectrics for use in applications, such as commercial aviation. Following the selection and modification of suitable thermoelectric materials, the function of the thermoelectric module in the specific environments should be optimized.

One strategy previously mentioned to be applied in RTGs is the use of segmented thermoelectric legs. Each material exhibits a peak in zT at varying temperature ranges, depending on the bandgap width. This limits its versatility in applications as this temperature range tends to be narrow, allowing the thermoelectric to shine only at the specific applications. Segmentation is performed to extend the peak performance of the thermoelectric leg to a wider temperature range as compared with each of the materials individually. Figure 8 depicts a schematic on how segmented thermoelectric legs are arranged in a module.

The multipart leg will comprise a material with a peak zT at only high and low temperatures individually. The material that performs best at high temperatures will be connected to the same side as the heat source, while the material for lower operating temperatures will be near the heat sink. As the heat source supplies thermal energy to TE #1 and taking into consideration the insulating layer and the intrinsic thermal conductivity of the material, some heat will be conducted to the interface of TE #1 and TE #2. Hence, one end of material TE #2 will be heated, but to a lower temperature as compared with direct heating from the source. This imposes different temperature gradients across each material, allowing them to operate at their optimal conditions.

In terms of zT, using a single material leg will allow the TE to perform best at a narrow temperature range (as shown by the corresponding dashed graphs). However, segmentation allows for the combination of strengths of the constituent materials, thus increasing the average zT (black solid line) and viable operating temperature of the thermoelectric.

This segmentation technique has been used in RTG modules to maximize power conversion. Taking the example of Si-based materials, the peak zT occurs at temperatures above 900 °C. At lower temperatures, the zT could decrease to as low as half the maximum value. Through segmentation with other thermoelectrics, such as skutterudites or PbTe, the peak zT is broadened across a larger temperature range, which would allow for more effective energy harvesting as the heat source diminishes over time.

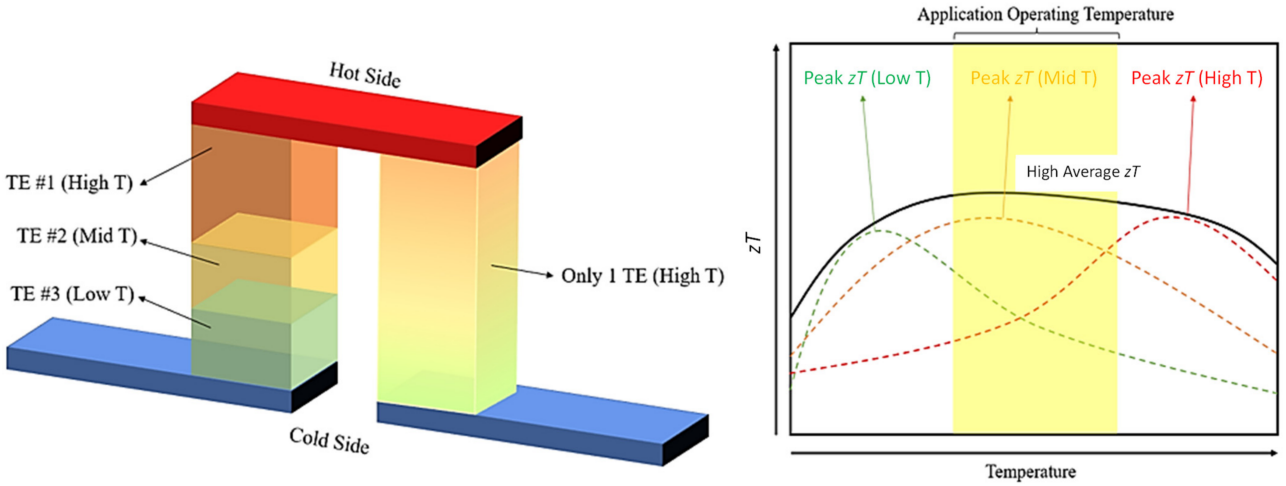

Figure 8. Segmented thermoelectric legs improve the average zT across a wider temperature range in comparison with single material legs.

However, using multiple components will introduce additional considerations. Apart from the electrode contact resistance, which is also examined in single material thermoelectric legs, the electrode–electrode resistance should also be considered for segmented thermoelectric legs. Additionally, to achieve the optimal zT, the relative current density $u = J/\kappa\nabla T$ of the segments should be equal to the compatibility factors as defined by $s = \left(\sqrt{1+zT}-1\right)/ST$ [94]. Since the relative current density is the ratio of the electric current density to the heat flux by conduction, and the compatibility factor is similarly a ratio of the figure of merit to the Seebeck coefficient, high values imply a good individual thermoelectric performance. However, as a part of a segmented leg, it is ideal for the materials to have similar current densities and compatibility factors to have an efficient thermoelectric generator. The guideline for selecting appropriate materials is to have the compatibility factors differ by less than a factor of 2. Otherwise, the efficiency of the segmented material may decrease instead.

In his work, Snyder et al. reiterates the effectiveness of segmented thermoelectric legs in RTGs. The material used for the lower temperature range was TAGS $((AgSbTe_2)_{0.15}(GeTe)_{0.85}$, operating below 525 °C, while PbTe was used for the temperature range above 600 °C for the n-type leg. In selecting the appropriate materials for the p-type leg, Snyder used TAGS as the reference material to be a part of the leg. Comparing the performances of various materials, the zT of PbTe matches more to TAGS as compared with SnTe, which exhibits a much lower zT at the required operational temperature [149]. However, upon comparison of the compatibility factor, the graph for PbTe drops much lower than that for SnTe, making SnTe the more suitable candidate for segmentation with TAGS at the 525–600 °C temperature range, and his results support this pairing, which has a higher efficiency than the PbTe–TAGS pair.

Similarly, for ATEGs, segmentation is also possible and was discussed in this paper by Shen et al. [110]. Currently, the study of segmented annular TEGs (SATEGs) is less developed compared with its flat counterpart and is deserving of more attention, especially for studies approaching from a device point of view.

Alternative to segmentation, other methods have been explored to increase the performance of TEGs across a wider temperature range. Interestingly, a recent paper by Niu et al. discussed the use of functionally graded materials (FGMs) in ATEGs [150]. For functionally graded materials, the dopant concentration is tailored to be different across the thermoelectric leg such that the Seebeck coefficient increases from the cold end to the hot end. This was suggested as an alternative to segmentation to avoid problems regarding delamination or material compatibility. FGMs for silicon-based materials were previously studied by Hedegaard et al. and Rogolino et al. as well, although no studies have yet explored the performance of the material in an ATEG [151,152].

5.2. Environmental and Situational Considerations

It is important to note that additional considerations should also be in place depending on the environment and situation that the thermoelectric module is utilized in. For commercial planes, there are multiple possible locations to install thermoelectric devices–the most common being the fuselage, where low-temperature thermoelectrics are utilized for powering WSNs [153,154]. Looking toward further usage of thermoelectrics in commercial aviation, models have been constructed around the installation of thermoelectric generators at the plane engine nozzles [109]. As previously mentioned, the temperature gradient in this area can be large. Hence, thermoelectric materials of wide bandgaps and a high melting point are required to tolerate the operating temperature of the engine.

To begin exploring the possibility of using TEGs in other areas of the plane, a sufficient area should be available, and the weight penalty incurred from the installation should not outweigh the potential benefits of the TEG. In addition, the ambient temperature at a cruising altitude poses the problem of icing. When the temperature increases during descent, the melted ice may cause water damage to the thermoelectric device if not adequately protected. The issue of short circuit due to liquid is also faced constantly with changes in humidity and precipitation. Moreover, the area near the engine is vulnerable to mechanical vibrations and drastic pressure changes. It is of utmost importance to ensure the secure adhesion of the device onto the surface and to conduct cyclic mechanical and thermal testing before releasing the application for commercial use. Ideally, the TEG would utilize a substrate that can conform to the curvature of the planes' surface to prevent strain during expansion and contraction of the components.

Concerning the cost, it is important to consider the longevity of the TEG as the life cycle of commercial planes is on average 30 years. The developments of new materials should also be noted to forecast any required upgrade in device. While waste heat harvesting has its financial gains, the transit to launching its widescale use could be challenging due to the high start-up costs and the required certification from the Federal Aviation Administration.

Similarly, for RTGs as the operating temperature can be extremely high up to 1273 K for GPHS-RTG, as shown in Table 1, thermoelectric materials of wide bandgaps and high melting points are also required. In addition, thermoelectric modules utilized in RTGs need to be mechanically robust to endure the harsh entry and landing conditions.

6. Conclusions and Outlooks

The large temperature difference and multiple possible applications that can be powered by scavenged energy make thermoelectrics an ideal match for use in commercial aviation. Further development of existing materials, such as upcycled silicon, could bring more value to TEGs, especially due to its light weight and crust abundance. In addition, with the advancement of small-scale devices, such as self-powered sensors, for low-temperature applications, the time is ripe to translate the benefits to harvest heat for high-temperature applications. For example, Wahbah et al. utilized a 9 cm^2 TEG to generate 20 μW at 22 K.

Due to the relation of TEG efficiency to the Carnot cycle, a better conversion efficiency can be expected at high-temperature environments. Waste heat harvesting can bring about economic and environmental benefits, and thermoelectric cooling can also delay the degradation of equipment. Having realized the energy generation potential in commercial aviation, more studies have been conducted in recent years to capitalize on this opportunity. Similarly, well-studied RTG technologies are continuously being developed to maximize the power harvested from scarce radioisotopes. Although the large temperature gradients paint an optimistic picture for efficient energy generation, multiple factors still need to be considered when designing TEGs for specific applications, which will be tested by various other elements, such as air pressure, humidity, and mechanical stress. Nevertheless, it is a worthwhile investment to research thermoelectrics for high-temperature applications as a long-term solution for sustainable energy generation.

Author Contributions: All authors (S.S.F.D., D.Z., W.Y.S.L., J.C., H.L., Q.Z., C.K.I.T., J.X., X.J.L. and A.S.) contributed to the writing; S.S.F.D. and A.S. contributed to the organization of materials and sections. All authors have read and agreed to the published version of the manuscript.

Funding: This work was supported by Singapore Aerospace Programme Cycle 15, grant number M2115a0092, Agency for Science, Technology, and Research (A*STAR); Singapore Career Development Fund (CDF), grant number C210112022; and Sustainable Hybrid Lighting System for Controlled Environment Agriculture Program, grant number A19D9a0096.

Institutional Review Board Statement: Not applicable.

Informed Consent Statement: Not applicable.

Data Availability Statement: Not applicable.

Conflicts of Interest: The authors declare no competing financial interests and the authors declare no conflict of interest.

References

1. Global Change Data Lab. Available online: https://ourworldindata.org/explorers/energy?tab=table&time=2009..latest&country=USA~{}GBR~{}CHN~{}OWID_WRL~{}IND~{}BRA~{}ZAF&Total+or+Breakdown=Total&Energy+or+Electricity=Primary+energy&Metric=Annual+consumption (accessed on 1 December 2021).
2. Benghanem, M.; Al-Mashraqi, A.A.; Daffallah, K.O. Performance of solar cells using thermoelectric module in hot sites. *Renew. Energy* **2016**, *89*, 51–59. [CrossRef]
3. Mazareanu, E. Total Fuel Consumption of Commercial Airlines Worldwide between 2005 and 2021. Available online: https://www.statista.com/statistics/655057/fuel-consumption-of-airlines-worldwide/ (accessed on 6 January 2022).
4. Wang, B.; Zheng, S.; Chen, Y.; Wang, Q.; Li, Z.; Wu, Y.; Li, J.; Mu, Y.; Xu, S.; Liang, J. Realizing ultralow thermal conductivity in Cu3SbSe4 via all-scale phonon scattering by co-constructing multiscale heterostructure and IIIB element doping. *Mater. Today Energy* **2021**, *19*, 100620. [CrossRef]
5. Wu, M.; Yao, K.; Li, D.; Huang, X.; Liu, Y.; Wang, L.; Song, E.; Yu, J.; Yu, X. Self-powered skin electronics for energy harvesting and healthcare monitoring. *Mater. Today Energy* **2021**, *21*, 100786. [CrossRef]
6. Xin, C.; Hu, Z.; Fang, Z.; Chaudhary, M.; Xiang, H.; Xu, X.; Aigouy, L.; Chen, Z. Flexible and wearable plasmonic-enabled organic/inorganic hybrid photothermoelectric generators. *Mater. Today Energy* **2021**, *22*, 100859. [CrossRef]
7. Zheng, Z.-H.; Wang, T.; Yang, D.; Jabar, B.; Abbas, A.; Li, F.; Chen, Y.-X.; Zha, X.-H.; Liang, G.-X.; Fan, P. Nanostructural manipulations for achieving record-high room temperature figure of merit in the ZnSb thin films. *Mater. Today Energy* **2021**, *22*, 100870. [CrossRef]
8. Suwardi, A.; Wang, F.; Xue, K.; Han, M.; Teo, P.; Wang, P.; Wang, S.; Liu, Y.; Ye, E.; Li, Z.; et al. Machine Learning-Driven Biomaterials Evolution. *Adv. Mater.* **2021**, *34*, 2102703. [CrossRef]
9. Zhang, D.; Duran, S.S.F.; Lim, W.Y.S.; Tan, C.K.I.; Cheong, W.C.D.; Suwardi, A.; Loh, X.J. SARS-CoV-2 in wastewater: From detection to evaluation. *Mater. Today Adv.* **2022**, *13*, 100211. [CrossRef] [PubMed]
10. Zhu, B.; Su, X.; Shu, S.; Luo, Y.; Tan, X.Y.; Sun, J.; Sun, D.; Zhang, H.; Zhang, Q.; Suwardi, A.; et al. Cold-Sintered Bi2Te3-Based Materials for Engineering Nanograined Thermoelectrics. *ACS Appl. Energy Mater.* **2022**. [CrossRef]
11. He, J.; Tritt, T.M. Advances in thermoelectric materials research: Looking back and moving forward. *Science* **2017**, *357*, eaak9997. [CrossRef] [PubMed]
12. Tan, G.; Zhao, L.-D.; Kanatzidis, M.G. Rationally Designing High-Performance Bulk Thermoelectric Materials. *Chem. Rev.* **2016**, *116*, 12123–12149. [CrossRef] [PubMed]
13. Zhu, J.; Zhou, C.; Zhang, M. Recent progress in flexible tactile sensor systems: From design to application. *Soft Sci.* **2021**, *1*, 3. [CrossRef]
14. Lim, W.Y.S.; Zhang, D.; Duran, S.S.F.; Tan, X.Y.; Tan, C.K.I.; Xu, J.; Suwardi, A. Physical Intuition to Improve Electronic Properties of Thermoelectrics. *Front. Phys.* **2021**, *9*, 683. [CrossRef]
15. Zhao, Y.; Zheng, M.; Wu, J.; Guan, X.; Suwardi, A.; Li, Y.; Lal, M.; Xie, G.; Zhang, G.; Zhang, L.; et al. Modification of thermal transport in few-layer MoS 2 by atomic-level defect engineering. *Nanoscale* **2021**, *13*, 11561–11567. [CrossRef] [PubMed]
16. Jia, N.; Cao, J.; Tan, X.Y.; Zheng, J.; Chien, S.W.; Yang, L.; Chen, K.; Ng, H.K.; Duran, S.S.F.; Liu, H.; et al. Suppressing Ge-vacancies to achieve high single-leg efficiency in GeTe with an ultra-high room temperature power factor. *J. Mater. Chem. A* **2021**, *9*, 23335–23344. [CrossRef]
17. Png, Z.M.; Soo, X.Y.D.; Chua, M.H.; Ong, P.J.; Suwardi, A.; Tan, C.K.I.; Xu, J.; Zhu, Q. Strategies to reduce the flammability of organic phase change Materials: A review. *Sol. Energy* **2021**, *231*, 115–128. [CrossRef]
18. Sun, H.-L.; Yang, C.-L.; Wang, M.-S.; Ma, X.-G.; Yi, Y.-G. High thermoelectric efficiency fluoride perovskite materials of AgMF3 (M = Zn, Cd). *Mater. Today Energy* **2021**, *19*, 100611. [CrossRef]

19. Ivanov, Y.; Levin, A.A.; Novikov, S.; Pshenay-Severin, D.; Volkov, M.; Zyuzin, A.; Burkov, A.; Nakama, T.; Schnatmann, L.; Reith, H.; et al. Low-temperature thermal conductivity of thermoelectric Co1− xMxSi (M= Fe, Ni) alloys. *Mater. Today Energy* **2021**, *20*, 100666. [CrossRef]
20. Lee, K.; Kim, Y.-M.; Park, C.; Shin, W.; Kim, S.; Kim, H.-S. Cumulative defect structures for experimentally attainable low thermal conductivity in thermoelectric (Bi,Sb)2Te3 alloys. *Mater. Today Energy* **2021**, *21*, 100795. [CrossRef]
21. Li, J.M.; Ming, H.W.; Song, C.J.; Wang, L.; Xin, H.X.; Gu, Y.J.; Zhang, J.; Qin, X.Y.; Li, D. Synergetic modulation of power factor and thermal conductivity for Cu3SbSe4-based system. *Mater. Today Energy* **2020**, *18*, 100491. [CrossRef]
22. Heremans, J.P.; Jovovic, V.; Toberer, E.S.; Saramat, A.; Kurosaki, K.; Charoenphakdee, A.; Yamanaka, S.; Snyder, G.J. Enhancement of Thermoelectric Efficiency in PbTe by Distortion of the Electronic Density of States. *Science* **2008**, *321*, 554–557. [CrossRef] [PubMed]
23. Zhang, X.; Shen, J.; Lin, S.; Li, J.; Chen, Z.; Li, W.; Pei, Y. Thermoelectric properties of GeSe. *J. Mater.* **2016**, *2*, 331–337. [CrossRef]
24. Bourgès, C.; Srinivasan, B.; Fontaine, B.; Sauerschnig, P.; Minard, A.; Halet, J.-F.; Miyazaki, Y.; Berthebaud, D.; Mori, T. Tailoring the thermoelectric and structural properties of Cu–Sn based thiospinel compounds [CuM1+xSn1−xS4 (M = Ti, V, Cr, Co)]. *J. Mater. Chem. C* **2020**, *8*, 16368–16383. [CrossRef]
25. Muchtar, A.R.; Srinivasan, B.; Le Tonquesse, S.; Singh, S.; Soelami, N.; Yuliarto, B.; Berthebaud, D.; Mori, T. Physical Insights on the Lattice Softening Driven Mid-Temperature Range Thermoelectrics of Ti/Zr-Inserted SnTe—An Outlook Beyond the Horizons of Conventional Phonon Scattering and Excavation of Heikes' Equation for Estimating Carrier Properties. *Adv. Energy Mater.* **2021**, *11*, 2101122. [CrossRef]
26. Srinivasan, B.; Berthebaud, D.; Mori, T. Is LiI a Potential Dopant Candidate to Enhance the Thermoelectric Performance in Sb-Free GeTe Systems? A Prelusive Study. *Energies* **2020**, *13*, 643. [CrossRef]
27. Srinivasan, B.; Cui, S.; Prestipino, C.; Gellé, A.; Boussard-Pledel, C.; Ababou-Girard, S.; Trapananti, A.; Bureau, B.; Di Matteo, S. Possible Mechanism for Hole Conductivity in Cu–As–Te Thermoelectric Glasses: A XANES and EXAFS Study. *J. Phys. Chem. C* **2017**, *121*, 14045–14050. [CrossRef]
28. Srinivasan, B.; Fontaine, B.; Gucci, F.; Dorcet, V.; Saunders, T.G.; Yu, M.; Cheviré, F.; Boussard-Pledel, C.; Halet, J.-F.; Gautier, R.; et al. Effect of the Processing Route on the Thermoelectric Performance of Nanostructured CuPb18SbTe20. *Inorg. Chem.* **2018**, *57*, 12976–12986. [CrossRef] [PubMed]
29. Srinivasan, B.; Gellé, A.; Gucci, F.; Boussard-Pledel, C.; Fontaine, B.; Gautier, R.; Halet, J.-F.; Reece, M.J.; Bureau, B. Realizing a stable high thermoelectric zT $\sim$ 2 over a broad temperature range in Ge1−x−yGaxSbyTe via band engineering and hybrid flash-SPS processing. *Inorg. Chem. Front.* **2019**, *6*, 63–73. [CrossRef]
30. Srinivasan, B.; Le Tonquesse, S.; Gellé, A.; Bourgès, C.; Monier, L.; Ohkubo, I.; Halet, J.-F.; Berthebaud, D.; Mori, T. Screening of transition (Y, Zr, Hf, V, Nb, Mo, and Ru) and rare-earth (La and Pr) elements as potential effective dopants for thermoelectric GeTe – an experimental and theoretical appraisal. *J. Mater. Chem. A* **2020**, *8*, 19805–19821. [CrossRef]
31. Virtudazo, R.V.R.; Srinivasan, B.; Guo, Q.; Wu, R.T.; Takei, T.; Shimasaki, Y.; Wada, H.; Kuroda, K.; Bernik, S.; Mori, T. Improvement in the thermoelectric properties of porous networked Al-doped ZnO nanostructured materials synthesized via an alternative interfacial reaction and low-pressure SPS processing. *Inorg. Chem. Front.* **2020**, *7*, 4118–4132. [CrossRef]
32. Camut, J.; Pham, N.; Truong, D.N.; Castillo-Hernandez, G.; Farahi, N.; Yasseri, M.; Mueller, E.; de Boor, J. Aluminum as promising electrode for Mg2(Si,Sn)-based thermoelectric devices. *Mater. Today Energy* **2021**, *21*, 100718. [CrossRef]
33. Du, Y.; Xu, J.; Paul, B.; Eklund, P. Flexible thermoelectric materials and devices. *Appl. Mater. Today* **2018**, *12*, 366–388. [CrossRef]
34. Huang, X.-L.; Ao, D.-W.; Chen, T.-B.; Chen, Y.-X.; Li, F.; Chen, S.; Liang, G.-X.; Zhang, X.-H.; Zheng, Z.-H.; Fan, P. High-performance copper selenide thermoelectric thin films for flexible thermoelectric application. *Mater. Today Energy* **2021**, *21*, 100743. [CrossRef]
35. Xue, K.; Wang, F.; Suwardi, A.; Han, M.-Y.; Teo, P.; Wang, P.; Wang, S.; Ye, E.; Li, Z.; Loh, X.J. Biomaterials by design: Harnessing data for future development. *Mater. Today Bio* **2021**, *12*, 100165. [CrossRef]
36. Lin, J.; Ma, L.; Liu, Q.; Xie, K.; Hu, Y.; Zhang, L.; Li, S.; Lu, M.; Qiao, G. Continuous phase transition in thermoelectric Zn_4Sb_3. *Mater. Today Energy* **2021**, *21*, 100787. [CrossRef]
37. Liu, E.; Negm, A.; Howlader, M. Thermoelectric generation via tellurene for wearable applications: Recent advances, research challenges, and future perspectives. *Mater. Today Energy* **2021**, *20*, 100625. [CrossRef]
38. Maksymuk, M.; Parashchuk, T.; Dzundza, B.; Nykyruy, L.; Chernyak, L.; Dashevsky, Z. Highly efficient bismuth telluride–based thermoelectric microconverters. *Mater. Today Energy* **2021**, *21*, 100753. [CrossRef]
39. Fu, C.; Wu, H.; Liu, Y.; He, J.; Zhao, X.; Zhu, T. Enhancing the Figure of Merit of Heavy-Band Thermoelectric Materials Through Hierarchical Phonon Scattering. *Adv. Sci.* **2016**, *3*, 1600035. [CrossRef]
40. Zheng, Y.; Slade, T.J.; Hu, L.; Tan, X.Y.; Luo, Y.; Luo, Z.-Z.; Xu, J.; Yan, Q.; Kanatzidis, M.G. Defect engineering in thermoelectric materials: What have we learned? *Chem. Soc. Rev.* **2021**, *50*, 9022–9054. [CrossRef] [PubMed]
41. Sharma, P.K.; Senguttuvan, T.; Sharma, V.K.; Chaudhary, S. Revisiting the thermoelectric properties of lead telluride. *Mater. Today Energy* **2021**, *21*, 100713. [CrossRef]
42. Tang, S.; Bai, S.; Wu, M.; Luo, D.; Wang, D.; Yang, S.; Zhao, L.-D. Honeycomb-like puckered PbSe with wide bandgap as promising thermoelectric material: A first-principles prediction. *Mater. Today Energy* **2021**, *23*, 100914. [CrossRef]
43. Zhang, W.; Li, X.; Zou, R.; Wu, H.; Shi, H.; Yu, S.; Liu, Y. Multifunctional glucose biosensors from Fe3O4 nanoparticles modified chitosan/graphene nanocomposites. *Sci. Rep.* **2015**, *5*, 11129. [CrossRef] [PubMed]

44. Xu, T.; Haruna, A.-Y.; Ma, Z.; Li, W.; Li, J.; Luo, Y.; Zhang, D.; Yang, J. High Power Factor and Thermoelectric Figure of Merit in Sb2Si2Te6 through Synergetic Effect of Ca Doping. *Chem. Mater.* **2021**, *33*, 8097–8105. [CrossRef]
45. Ramesh, V.P.; Sargolzaeiaval, Y.; Neumann, T.; Misra, V.; Vashaee, D.; Dickey, M.D.; Ozturk, M.C. Flexible thermoelectric generator with liquid metal interconnects and low thermal conductivity silicone filler. *npj Flex. Electron.* **2021**, *5*, 5. [CrossRef]
46. Luo, Y.; Xu, T.; Ma, Z.; Zhang, D.; Guo, Z.; Jiang, Q.; Yang, J.; Yan, Q.; Kanatzidis, M.G. Cubic AgMnSbTe3 Semiconductor with a High Thermoelectric Performance. *J. Am. Chem. Soc.* **2021**, *143*, 13990–13998. [CrossRef] [PubMed]
47. Hu, L.; Luo, Y.; Fang, Y.; Qin, F.; Cao, X.; Xie, H.; Liu, J.; Dong, J.; Sanson, A.; Giarola, M.; et al. High Thermoelectric Performance through Crystal Symmetry Enhancement in Triply Doped Diamondoid Compound Cu_2SnSe_3. *Adv. Energy Mater.* **2021**, *11*, 2100661. [CrossRef]
48. Hu, L.; Fang, Y.-W.; Qin, F.; Cao, X.; Zhao, X.; Luo, Y.; Repaka, D.V.M.; Luo, W.; Suwardi, A.; Soldi, T.; et al. High thermoelectric performance enabled by convergence of nested conduction bands in $Pb_7Bi_4Se_{13}$ with low thermal conductivity. *Nat. Commun.* **2021**, *12*, 4793. [CrossRef]
49. Luo, Y.; Hao, S.; Cai, S.; Slade, T.J.; Luo, Z.Z.; Dravid, V.P.; Wolverton, C.; Yan, Q.; Kanatzidis, M.G. High Thermoelectric Performance in the New Cubic Semiconductor $AgSnSbSe_3$ by High-Entropy Engineering. *J. Am. Chem. Soc.* **2020**, *142*, 15187–15198. [CrossRef] [PubMed]
50. Luo, Y.; Cai, S.; Hao, S.; Pielnhofer, F.; Hadar, I.; Luo, Z.-Z.; Xu, J.; Wolverton, C.; Dravid, V.P.; Pfitzner, A.; et al. High-Performance Thermoelectrics from Cellular Nanostructured $Sb_2Si_2Te_6$. *Joule* **2020**, *4*, 159–175. [CrossRef]
51. Zhang, D.; Lim, W.Y.S.; Duran, S.S.F.; Loh, X.J.; Suwardi, A. Additive Manufacturing of Thermoelectrics: Emerging Trends and Outlook. *ACS Energy Lett.* **2022**, *7*, 720–735. [CrossRef]
52. Cao, J.; Zheng, J.; Liu, H.; Tan, C.K.I.; Wang, X.; Wang, W.; Zhu, Q.; Li, Z.; Zhang, G.; Wu, J.; et al. Flexible Elemental Thermoelectrics with Ultra-high Power Density. *Mater. Today Energy* **2022**, 100964. [CrossRef]
53. Cao, J.; Tan, X.Y.; Jia, N.; Lan, D.; Solco, S.F.D.; Chen, K.; Chien, S.W.; Liu, H.; Tan, C.K.I.; Zhu, Q.; et al. Improved zT in Nb5Ge3–GeTe thermoelectric nanocomposite. *Nanoscale* **2021**, *14*, 410–418. [CrossRef] [PubMed]
54. Zhi, S.; Jia, J.; Zhang, Q.; Cao, F.; Liu, X.; Mao, J. A sketch for super-thermoelectric materials. *Mater. Today Phys.* **2022**, *22*, 100618. [CrossRef]
55. Hong, M.; Lyu, W.; Wang, Y.; Zou, J.; Chen, Z.-G. Establishing the Golden Range of Seebeck Coefficient for Maximizing Thermoelectric Performance. *J. Am. Chem. Soc.* **2020**, *142*, 2672–2681. [CrossRef]
56. Cao, J.; Chien, S.W.; Tan, X.Y.; Tan, C.K.I.; Zhu, Q.; Wu, J.; Wang, X.; Zhao, Y.; Yang, L.; Yan, Q.; et al. Realizing zT Values of 2.0 in Cubic GeTe. *ChemNanoMat* **2021**, *7*, 476–482. [CrossRef]
57. Qin, F.; Nikolaev, S.A.; Suwardi, A.; Wood, M.; Zhu, Y.; Tan, X.; Aydemir, U.; Ren, Y.; Yan, Q.; Hu, L.; et al. Crystal Structure and Atomic Vacancy Optimized Thermoelectric Properties in Gadolinium Selenides. *Chem. Mater.* **2020**, *32*, 10130–10139. [CrossRef]
58. Hari, V.; Rakovec, O.; Markonis, Y.; Hanel, M.; Kumar, R. Increased future occurrences of the exceptional 2018–2019 Central European drought under global warming. *Sci. Rep.* **2020**, *10*, 12207. [CrossRef] [PubMed]
59. Suwardi, A.; Cao, J.; Hu, L.; Wei, F.; Wu, J.; Zhao, Y.; Lim, S.H.; Yang, L.; Tan, X.Y.; Chien, S.W.; et al. Tailoring the phase transition temperature to achieve high-performance cubic GeTe-based thermoelectrics. *J. Mater. Chem. A* **2020**, *8*, 18880–18890. [CrossRef]
60. Suwardi, A.; Cao, J.; Zhao, Y.; Wu, J.; Chien, S.; Tan, X.; Hu, L.; Wang, X.; Wang, W.; Li, D.; et al. Achieving high thermoelectric quality factor toward high figure of merit in GeTe. *Mater. Today Phys.* **2020**, *14*, 100239. [CrossRef]
61. Suwardi, A.; Hu, L.; Wang, X.; Tan, X.Y.; Repaka, D.V.M.; Wong, L.-M.; Ni, X.; Liew, W.H.; Lim, S.H.; Yan, Q.; et al. Origin of High Thermoelectric Performance in Earth-Abundant Phosphide–Tetrahedrite. *ACS Appl. Mater. Interfaces* **2020**, *12*, 9150–9157. [CrossRef]
62. Tan, L.P.; Sun, T.; Fan, S.; Ng, L.Y.; Suwardi, A.; Yan, Q.; Hng, H.H. Facile synthesis of Cu7Te4 nanorods and the enhanced thermoelectric properties of Cu_7Te_4–$Bi_{0.4}Sb_{1.6}Te_3$ nanocomposites. *Nano Energy* **2013**, *2*, 4–11. [CrossRef]
63. Zheng, Y.; Xie, H.; Zhang, Q.; Suwardi, A.; Cheng, X.; Zhang, Y.; Shu, W.; Wan, X.; Yang, Z.; Liu, Z.; et al. Unraveling the Critical Role of Melt-Spinning Atmosphere in Enhancing the Thermoelectric Performance of p-Type $Bi_{0.52}Sb_{1.48}Te_3$ Alloys. *ACS Appl. Mater. Interfaces* **2020**, *12*, 36186–36195. [CrossRef] [PubMed]
64. Zhu, Q.; Wang, S.; Wang, X.; Suwardi, A.; Chua, M.H.; Soo, X.Y.D.; Xu, J. Bottom-Up Engineering Strategies for High-Performance Thermoelectric Materials. *Nano-Micro Lett.* **2021**, *13*, 119. [CrossRef] [PubMed]
65. Chang, C.; Wang, D.; He, D.; He, W.; Zhu, F.; Wang, G.; He, J.; Zhao, L. Realizing High-Ranged Out-of-Plane ZTs in N-Type SnSe Crystals through Promoting Continuous Phase Transition. *Adv. Energy Mater.* **2019**, *9*, 1901334. [CrossRef]
66. Luo, Y.; Cai, S.; Hua, X.; Chen, H.; Liang, Q.; Du, C.-F.; Zheng, Y.; Shen, J.; Xu, J.; Wolverton, C.; et al. High Thermoelectric Performance in Polycrystalline SnSe Via Dual-Doping with Ag/Na and Nanostructuring With Ag_8SnSe_6. *Adv. Energy Mater.* **2019**, *9*, 1803072. [CrossRef]
67. Luo, Y.; Zheng, Y.; Luo, Z.; Hao, S.; Du, C.-F.; Liang, Q.; Li, Z.; Khor, K.A.; Hippalgaonkar, K.; Xu, J.; et al. n-Type SnSe 2 Oriented-Nanoplate-Based Pellets for High Thermoelectric Performance. *Adv. Energy Mater.* **2018**, *8*, 1702167. [CrossRef]
68. Qin, B.; Zhang, Y.; Wang, D.; Zhao, Q.; Gu, B.; Wu, H.; Zhang, H.; Ye, B.; Pennycook, S.J.; Zhao, L.-D. Ultrahigh Average ZT Realized in p-Type SnSe Crystalline Thermoelectrics through Producing Extrinsic Vacancies. *J. Am. Chem. Soc.* **2020**, *142*, 5901–5909. [CrossRef]
69. Shi, X.-L.; Chen, W.-Y.; Zhang, T.; Zou, J.; Chen, Z.-G. Fiber-based thermoelectrics for solid, portable, and wearable electronics. *Energy Environ. Sci.* **2020**, *14*, 729–764. [CrossRef]

70. Roychowdhury, S.; Ghosh, T.; Arora, R.; Samanta, M.; Xie, L.; Singh, N.K.; Soni, A.; He, J.; Waghmare, U.V.; Biswas, K. Enhanced atomic ordering leads to high thermoelectric performance in $AgSbTe_2$. *Science* **2021**, *371*, 722–727. [CrossRef] [PubMed]
71. Mao, J.; Chen, G.; Ren, Z. Thermoelectric cooling materials. *Nat. Mater.* **2021**, *20*, 454–461. [CrossRef]
72. Liu, Z.; Sato, N.; Gao, W.; Yubuta, K.; Kawamoto, N.; Mitome, M.; Kurashima, K.; Owada, Y.; Nagase, K.; Lee, C.-H.; et al. Demonstration of ultrahigh thermoelectric efficiency of ~7.3% in Mg_3Sb_2/MgAgSb module for low-temperature energy harvesting. *Joule* **2021**, *5*, 1196–1208. [CrossRef]
73. Li, X.; Li, Z.; Chen, C.; Ren, Z.; Wang, C.; Liu, X.; Zhang, Q.; Chen, S. CALPHAD as a powerful technique for design and fabrication of thermoelectric materials. *J. Mater. Chem. A* **2021**, *9*, 6634–6649. [CrossRef]
74. Kozinsky, B.; Singh, D.J. Thermoelectrics by Computational Design: Progress and Opportunities. *Annu. Rev. Mater. Sci.* **2021**, *51*, 565–590. [CrossRef]
75. Suwardi, A.; Lim, S.H.; Zheng, Y.; Wang, X.; Chien, S.W.; Tan, X.Y.; Zhu, Q.; Wong, L.M.N.; Cao, J.; Wang, W.; et al. Effective enhancement of thermoelectric and mechanical properties of germanium telluride via rhenium-doping. *J. Mater. Chem. C* **2020**, *8*, 16940–16948. [CrossRef]
76. Dinh, K.N.; Sun, Y.; Pei, Z.; Yuan, Z.; Suwardi, A.; Huang, Q.; Liao, X.; Wang, Z.; Chen, Y.; Yan, Q. Electronic Modulation of Nickel Disulfide toward Efficient Water Electrolysis. *Small* **2020**, *16*, e1905885. [CrossRef]
77. Recatalà-Gómez, J.; Suwardi, A.; Nandhakumar, I.; Abutaha, A.; Hippalgaonkar, K. Toward Accelerated Thermoelectric Materials and Process Discovery. *ACS Appl. Energy Mater.* **2020**, *3*, 2240–2257. [CrossRef]
78. Suwardi, A.; Bash, D.; Ng, H.K.; Gomez, J.R.; Repaka, D.V.M.; Kumar, P.; Hippalgaonkar, K. Inertial effective mass as an effective descriptor for thermoelectrics via data-driven evaluation. *J. Mater. Chem. A* **2019**, *7*, 23762–23769. [CrossRef]
79. Suwardi, A.; Prasad, B.; Lee, S.; Choi, E.-M.; Lu, P.; Zhang, W.; Li, L.; Blamire, M.; Jia, Q.; Wang, H.; et al. Turning antiferromagnetic $Sm_{0.34}Sr_{0.66}MnO_3$ into a 140 K ferromagnet using a nanocomposite strain tuning approach. *Nanoscale* **2016**, *8*, 8083–8090. [CrossRef]
80. Wang, X.; Suwardi, A.; Lim, S.L.; Wei, F.; Xu, J. Transparent flexible thin-film p–n junction thermoelectric module. *npj Flex. Electron.* **2020**, *4*, 19. [CrossRef]
81. Wang, X.; Suwardi, A.; Zheng, Y.; Zhou, H.; Chien, S.W.; Xu, J. Enhanced Thermoelectric Performance of Nanocrystalline Indium Tin Oxide Pellets by Modulating the Density and Nanoporosity Via Spark Plasma Sintering. *ACS Appl. Nano Mater.* **2020**, *3*, 10156–10165. [CrossRef]
82. Xie, H.; Su, X.; Bailey, T.P.; Zhang, C.; Liu, W.; Uher, C.; Tang, X.; Kanatzidis, M.G. Anomalously Large Seebeck Coefficient of CuFeS2 Derives from Large Asymmetry in the Energy Dependence of Carrier Relaxation Time. *Chem. Mater.* **2020**, *32*, 2639–2646. [CrossRef]
83. Xiao, Y.; Zhao, L.-D. Seeking new, highly effective thermoelectrics. *Science* **2020**, *367*, 1196–1197. [CrossRef]
84. Wu, Y.; Liu, F.; Zhang, Q.; Zhu, T.; Xia, K.; Zhao, X. Enhancing the average thermoelectric figure of merit of elemental Te by suppressing grain boundary scattering. *J. Mater. Chem. A* **2020**, *8*, 8455–8461. [CrossRef]
85. Li, C.; Ma, S.; Wei, P.; Zhu, W.; Nie, X.; Sang, X.; Sun, Z.; Zhang, Q.; Zhao, W. Magnetism-induced huge enhancement of the room-temperature thermoelectric and cooling performance of p-type BiSbTe alloys. *Energy Environ. Sci.* **2020**, *13*, 535–544. [CrossRef]
86. Hong, M.; Zheng, K.; Lyv, W.; Li, M.; Qu, X.; Sun, Q.; Xu, S.; Zou, J.; Chen, Z.-G. Computer-aided design of high-efficiency GeTe-based thermoelectric devices. *Energy Environ. Sci.* **2020**, *13*, 1856–1864. [CrossRef]
87. Gucci, F.; Saunders, T.G.; Srinivasan, B.; Cheviré, F.; Ferluccio, D.; Bos, J.-W.G.; Reece, M.J. Hybrid Flash-SPS of TiNiCu0.05Sn with reduced thermal conductivity. *J. Alloy. Compd.* **2020**, *837*, 155058. [CrossRef]
88. Fu, C.; Sun, Y.; Felser, C. Topological thermoelectrics. *APL Mater.* **2020**, *8*, 040913. [CrossRef]
89. Bayikadi, K.S.; Wu, C.T.; Chen, L.-C.; Chen, K.-H.; Chou, F.-C.; Sankar, R. Synergistic optimization of thermoelectric performance of Sb doped GeTe with a strained domain and domain boundaries. *J. Mater. Chem. A* **2020**, *8*, 5332–5341. [CrossRef]
90. Qiu, Y.; Jin, Y.; Wang, D.; Guan, M.; He, W.; Peng, S.; Liu, R.; Gao, X.; Zhao, L.-D. Realizing high thermoelectric performance in GeTe through decreasing the phase transition temperature via entropy engineering. *J. Mater. Chem. A* **2019**, *7*, 26393–26401. [CrossRef]
91. Mao, J.; Zhu, H.; Ding, Z.; Liu, Z.; Gamage, G.A.; Chen, G.; Ren, Z. High thermoelectric cooling performance of n-type Mg_3Bi_2-based materials. *Science* **2019**, *365*, 495–498. [CrossRef] [PubMed]
92. Luo, Z.-Z.; Cai, S.; Hao, S.; Bailey, T.P.; Su, X.; Spanopoulos, I.; Hadar, I.; Tan, G.; Luo, Y.; Xu, J.; et al. High Figure of Merit in Gallium-Doped Nanostructured n-Type PbTe-xGeTe with Midgap States. *J. Am. Chem. Soc.* **2019**, *141*, 16169–16177. [CrossRef]
93. Kumar, P.M.; Jagadeesh Babu, V.; Subramanian, A.; Bandla, A.; Thakor, N.; Ramakrishna, S.; Wei, H. The Design of a Thermoelectric Generator and Its Medical Applications. *Designs* **2019**, *3*, 22. [CrossRef]
94. Snyder, J. Application of the compatibility factor to the design of segmented and cascaded thermoelectric generators. *Appl. Phys. Lett.* **2004**, *84*, 2436–2438. [CrossRef]
95. Ni, J.E.; Case, E.D.; Schmidt, R.D.; Wu, C.-I.; Hogan, T.P.; Trejo, R.M.; Kirkham, M.J.; Lara-Curzio, E.; Kanatzidis, M.G. The thermal expansion coefficient as a key design parameter for thermoelectric materials and its relationship to processing-dependent bloating. *J. Mater. Sci.* **2013**, *48*, 6233–6244. [CrossRef]

96. Crane, D.; LaGrandeur, J.; Jovovic, V.; Ranalli, M.; Adldinger, M.; Poliquin, E.; Dean, J.; Kossakovski, D.; Mazar, B.; Maranville, C. TEG On-Vehicle Performance and Model Validation and What It Means for Further TEG Development. *J. Electron. Mater.* **2013**, *42*, 1582–1591. [CrossRef]
97. National Research Council. *The Airliner Cabin Environment and the Health of Passengers and Crew*; National Academies Press: Washington, DC, USA, 2002.
98. Air Transport Action Group, Facts & Figures. Available online: https://www.atag.org/facts-figures.html (accessed on 1 December 2021).
99. Overton, J. Fact Sheet The Growth in Greenhouse Gas Emissions from Commercial Aviation. Available online: https://www.eesi.org/papers/view/fact-sheet-the-growth-in-greenhouse-gas-emissions-from-commercial-aviation (accessed on 1 December 2021).
100. Huang, J. Aerospace and Aircraft Thermoelectric Applications. Available online: https://www1.eere.energy.gov/vehiclesandfuels/pdfs/thermoelectrics_app_2009/thursday/huang.pdf (accessed on 1 December 2021).
101. Becker, T.; Elefsiniotis, A.; Kiziroglou, M. Thermoelectric Energy Harvesting in Aircraft. In *Micro Energy Harvesting*; Briand, D., Yeatman, E., Roundy, S., Eds.; Wiley-VCH Verlag: Weinheim, Germany, 2015; pp. 415–434. [CrossRef]
102. Aerospace Vehicle Systems Institute, Wireless Avionics Intra-Communications. Available online: https://waic.avsi.aero/about/ (accessed on 1 December 2021).
103. Crane, D.T.; Koripella, C.R.; Jovović, V. Validating Steady-State and Transient Modeling Tools for High-Power-Density Thermoelectric Generators. *J. Electron. Mater.* **2012**, *41*, 1524–1534. [CrossRef]
104. Liu, X.; Cao, J.; Lai, S.; Yang, C.; Wu, H.; Xu, Y.-L. Energy efficient clustering for WSN-based structural health monitoring. In Proceedings of the 2011 Proceedings IEEE INFOCOM, Shanghai, China, 10–15 April 2011; pp. 2768–2776.
105. Yedavalli, R.K.; Belapurkar, R.K. Application of wireless sensor networks to aircraft control and health management systems. *J. Control Theory Appl.* **2011**, *9*, 28–33. [CrossRef]
106. Roach, D.P. Use of Comparative Vacuum Monitoring Sensors for Automated, Wireless Health Monitoring of Bridges and Infrastructure. In *Maintenance, Safety, Risk, Management and Life-Cycle Performance of Bridges*; CRC Press: Boca Raton, FL, USA, 2018; pp. 2747–2751.
107. Samson, D.; Kluge, M.; Becker, T.; Schmid, U. Energy harvesting for autonomous wireless sensor nodes in aircraft. *Procedia Eng.* **2010**, *5*, 1160–1163. [CrossRef]
108. Elefsiniotis, A.; Kokorakis, N.; Becker, T.; Schmid, U. A thermoelectric-based energy harvesting module with extended operational temperature range for powering autonomous wireless sensor nodes in aircraft. *Sens. Actuators A Phys.* **2014**, *206*, 159–164. [CrossRef]
109. Ziolkowski, P.; Zabrocki, K.; Müller, E. TEG Design for Waste Heat Recovery at an Aviation Jet Engine Nozzle. *Appl. Sci.* **2018**, *8*, 2637. [CrossRef]
110. Shen, Z.-G.; Liu, X.; Chen, S.; Wu, S.-Y.; Xiao, L.; Chen, Z.-X. Theoretical analysis on a segmented annular thermoelectric generator. *Energy* **2018**, *157*, 297–313. [CrossRef]
111. Hammel, T.; Bennett, R.; Otting, W.; Fanale, S. Multi-Mission Radioisotope Thermoelectric Generator (MMRTG) and Performance Prediction Model. In Proceedings of the 7th International Energy Conversion Engineering Conference, Denver, CO, USA, 2–5 August 2009; p. 4576.
112. Jiang, M. An Overview of Radioisotope Thermoelectric Generators. Available online: http://large.stanford.edu/courses/2013/ph241/jiang1/ (accessed on 1 December 2021).
113. Ambrosi, R.M.; Williams, H.; Watkinson, E.J.; Barco, A.; Mesalam, R.; Crawford, T.; Bicknell, C.; Samara-Ratna, P.; Vernon, D.; Bannister, N.; et al. European Radioisotope Thermoelectric Generators (RTGs) and Radioisotope Heater Units (RHUs) for Space Science and Exploration. *Space Sci. Rev.* **2019**, *215*, 55. [CrossRef]
114. June, D.F.W.; Zakrajsek, J.F. *NASA Special Session: Next-Generation Radioisotope Thermoelectric Generator (RTG) Discussion*; National Aeronautics and Space Administration: Washington, DC, USA, 2017.
115. Houtmann, J. Enhancing NASA's Multi-Mission Radioisotope Thermoelectric Generator Using Highly Efficient Thermoelectric Materials. *Maneto Undergrad. Res. J.* **2020**, *3*. [CrossRef]
116. Anderson, D.L. Chemical composition of the mantle. *J. Geophys. Res. Earth Surf.* **1983**, *88*, B41–B52. [CrossRef]
117. Encyclopedia Britannica. Encyclopedia Britannica, Silicon Chemical Element. Available online: https://www.britannica.com/science/silicon (accessed on 1 December 2021).
118. Kessler, V.; Gautam, D.; Hülser, T.; Spree, M.; Theissmann, R.; Winterer, M.; Wiggers, H.; Schierning, G.; Schmechel, R. Thermoelectric Properties of Nanocrystalline Silicon from a Scaled-Up Synthesis Plant. *Adv. Eng. Mater.* **2013**, *15*, 379–385. [CrossRef]
119. Zhu, T.; Yu, G.; Xu, J.; Wu, H.; Fu, C.; Liu, X.; He, J.; Zhao, X. The Role of Electron-Phonon Interaction in Heavily Doped Fine-Grained Bulk Silicons as Thermoelectric Materials. *Adv. Electron. Mater.* **2016**, *2*, 1600171. [CrossRef]
120. Bux, S.K.; Blair, R.G.; Gogna, P.K.; Lee, H.; Chen, G.; Dresselhaus, M.S.; Kaner, R.B.; Fleurial, J.-P. Nanostructured Bulk Silicon as an Effective Thermoelectric Material. *Adv. Funct. Mater.* **2009**, *19*, 2445–2452. [CrossRef]
121. Schierning, G.; Theissmann, R.; Stein, N.; Petermann, N.; Becker, A.; Engenhorst, M.; Kessler, V.; Geller, M.R.; Beckel, A.; Wiggers, H.; et al. Role of oxygen on microstructure and thermoelectric properties of silicon nanocomposites. *J. Appl. Phys.* **2011**, *110*, 113515. [CrossRef]

122. Claudio, T.; Stein, N.; Stroppa, D.G.; Klobes, B.; Koza, M.M.; Kudejova, P.; Petermann, N.; Wiggers, H.; Schierning, G.; Hermann, R.P. Nanocrystalline silicon: Lattice dynamics and enhanced thermoelectric properties. *Phys. Chem. Chem. Phys.* **2014**, *16*, 25701–25709. [CrossRef]
123. Stoetzel, J.; Schneider, T.; Mueller, M.M.; Kleebe, H.-J.; Wiggers, H.; Schierning, G.; Schmechel, R. Microstructure and thermoelectric properties of Si-WSi2 nanocomposites. *Acta Mater.* **2017**, *125*, 321–326. [CrossRef]
124. Heath, G.A.; Silverman, T.J.; Kempe, M.; Deceglie, M.; Ravikumar, D.; Remo, T.; Cui, H.; Sinha, P.; Libby, C.; Shaw, S.; et al. Research and development priorities for silicon photovoltaic module recycling to support a circular economy. *Nat. Energy* **2020**, *5*, 502–510. [CrossRef]
125. Bahrami, A.; Schierning, G.; Nielsch, K. Waste Recycling in Thermoelectric Materials. *Adv. Energy Mater.* **2020**, *10*, 1904159. [CrossRef]
126. Cai, B.; Pei, J.; Dong, J.; Zhuang, H.-L.; Gu, J.; Cao, Q.; Hu, H.; Lin, Z.; Li, J.-F. $(Bi,Sb)_2Te_3$/SiC nanocomposites with enhanced thermoelectric performance: Effect of SiC nanoparticle size and compositional modulation. *Sci. China Mater.* **2021**, *64*, 2551–2562. [CrossRef]
127. Cai, B.; Zhuang, H.-L.; Pei, J.; Su, B.; Li, J.-W.; Hu, H.; Jiang, Y. Spark plasma sintered Bi-Sb-Te alloys derived from ingot scrap: Maximizing thermoelectric performance by tailoring their composition and optimizing sintering time. *Nano Energy* **2021**, *85*, 106040. [CrossRef]
128. Bose, S.; Acharya, H.N.; Banerjee, H.D. Electrocal, thermal, thermoelectric and related properties of magnesium silicide semiconductor prepared from rice husk. *J. Mater. Sci.* **1993**, *28*, 5461–5468. [CrossRef]
129. Bose, S. Thermal Conductivity of Magnesium Silicide Semiconductor Prepared from Rice Husk. *Phys. Status Solidi* **1992**, *129*, 127–134. [CrossRef]
130. He, R.; Heyn, W.; Thiel, F.; Pérez, N.; Damm, C.; Pohl, D.; Rellinghaus, B.; Reimann, C.; Beier, M.; Friedrich, J.; et al. Thermoelectric properties of silicon and recycled silicon sawing waste. *J. Mater.* **2019**, *5*, 15–33. [CrossRef]
131. Moen, M.; Halvorsen, T.; Mørk, K.; Velken, S. Recycling of silicon metal powder from industrial powder waste streams. *Met. Powder Rep.* **2017**, *72*, 182–187. [CrossRef]
132. Isoda, Y.; Tada, S.; Kitagawa, H.; Shinohara, Y. Thermoelectric Properties of Sb-Doped Mg2Si Prepared Using Different Silicon Sources. *J. Electron. Mater.* **2016**, *45*, 1772–1778. [CrossRef]
133. Mesaritis, G.; Symeou, E.; Delimitis, A.; Oikonomidis, S.; Jaegle, M.; Tarantik, K.; Nicolaou, C.; Kyratsi, T. Recycling Si-kerf from photovoltaics: A very promising route to thermoelectrics. *J. Alloy. Compd.* **2019**, *775*, 1036–1043. [CrossRef]
134. Britannica. Germanium Properties. Available online: https://www.britannica.com/science/germanium (accessed on 1 December 2021).
135. Dismukes, J.P.; Ekstrom, L.; Paff, R.J. Lattice Parameter and Density in Germanium-Silicon Alloys. *J. Phys. Chem.* **1964**, *68*, 3021–3027. [CrossRef]
136. Basu, R.; Singh, A. High temperature Si–Ge alloy towards thermoelectric applications: A comprehensive review. *Mater. Today Phys.* **2021**, *21*, 100468. [CrossRef]
137. Virginia Semiconductor. The General Properties of Si, Ge, SiGe, SiO_2 and Si_3N_4. Available online: https://studylib.net/doc/18232119/the-general-properties-of-si--ge--sige--sio2-and-si3n4 (accessed on 1 December 2021).
138. Taborda, J.A.P.; Rojo, M.M.; Maiz, J.; Neophytou, N.; Martin-Gonzalez, M. Ultra-low thermal conductivities in large-area Si-Ge nanomeshes for thermoelectric applications. *Sci. Rep.* **2016**, *6*, 32778. [CrossRef]
139. Hosseini, S.A.; Romano, G.; Greaney, P.A. Enhanced Thermoelectric Performance of Polycrystalline $Si_{0.8}Ge_{0.2}$ Alloys through the Addition of Nanoscale Porosity. *Nanomater.* **2021**, *11*, 2591. [CrossRef]
140. Gao, Z.; Lu, C.; Wang, Y.; Yang, S.; Yu, Y.; He, H. Super Stable Ferroelectrics with High Curie Point. *Sci. Rep.* **2016**, *6*, 24139. [CrossRef] [PubMed]
141. Zebarjadi, M.; Joshi, G.; Zhu, G.; Yu, B.; Minnich, A.; Lan, Y.; Wang, X.; Dresselhaus, M.; Ren, Z.; Chen, G. Power Factor Enhancement by Modulation Doping in Bulk Nanocomposites. *Nano Lett.* **2011**, *11*, 2225–2230. [CrossRef] [PubMed]
142. Pei, Y.-L.; Wu, H.; Wu, D.; Zheng, F.; He, J. High Thermoelectric Performance Realized in a BiCuSeO System by Improving Carrier Mobility through 3D Modulation Doping. *J. Am. Chem. Soc.* **2014**, *136*, 13902–13908. [CrossRef] [PubMed]
143. Yu, B.; Zebarjadi, M.; Wang, H.; Lukas, K.; Wang, H.; Wang, D.; Opeil, C.; Dresselhaus, M.; Chen, G.; Ren, Z. Enhancement of Thermoelectric Properties by Modulation-Doping in Silicon Germanium Alloy Nanocomposites. *Nano Lett.* **2012**, *12*, 2077–2082. [CrossRef] [PubMed]
144. Acharya, N.; Pawar, H.; Sanyal, S.P. Structural stability, electronic and thermoelectric properties of ruthenium silicide. *J. Alloy. Compd.* **2020**, *826*, 154164. [CrossRef]
145. Vining, C.B. Extrapolated thermoelectric figure of merit of ruthenium silicide. *AIP Conf. Proc.* **1992**, *246*, 338–342. [CrossRef]
146. Sawade, Y.; Ohta, T.; Yamamoto, A.; Tanaka, T.; Kamisako, K. Large thermoelectric figure of merit value of undoped polycrystalline ruthenium sesquisilicide. *AIP Conf. Proc.* **1994**, *316*, 99–104. [CrossRef]
147. Krivosheev, A.E.; Ivanenko, L.I.; Filonov, A.B.; Shaposhnikov, V.; Behr, G.; Schumann, J.; Borisenko, V. Thermoelectric efficiency of single crystal semiconducting ruthenium silicide. *Semiconductors* **2006**, *40*, 27–32. [CrossRef]
148. Nozariasbmarz, A.; Agarwal, A.; Coutant, Z.; Hall, M.J.; Liu, J.; Liu, R.; Malhotra, A.; Norouzzadeh, P.; Öztürk, M.C.; Ramesh, V.P.; et al. Thermoelectric silicides: A review. *Jpn. J. Appl. Phys.* **2017**, *56*, 05DA04. [CrossRef]

149. Snyder, J.; Caillat, T. Using the Compatibility Factor to Design High Efficiency Segmented Thermoelectric Generators. *MRS Proc.* **2003**, *793*, S2.1. [CrossRef]
150. Niu, W.; Cao, X.; Hu, Y.; Wang, F.; Shi, J. Theoretical analysis of annular thermoelectric generators made of functionally graded materials. *AIP Adv.* **2021**, *11*, 025333. [CrossRef]
151. Hedegaard, E.M.J.; Johnsen, S.; Bjerg, L.; Borup, K.A.; Iversen, B.B. Functionally Graded Ge1–xSix Thermoelectrics by Simultaneous Band Gap and Carrier Density Engineering. *Chem. Mater.* **2014**, *26*, 4992–4997. [CrossRef]
152. Rogolino, P.; Cimmelli, V.A. Thermoelectric Efficiency of Silicon–Germanium Alloys in Finite-Time Thermodynamics. *Entropy* **2020**, *22*, 1116. [CrossRef] [PubMed]
153. Samson, D.; Kluge, M.; Fuss, T.; Schmid, U.; Becker, T. Flight Test Results of a Thermoelectric Energy Harvester for Aircraft. *J. Electron. Mater.* **2012**, *41*, 1134–1137. [CrossRef]
154. Jia, Y.; Jiang, Q.; Sun, H.; Liu, P.; Hu, D.; Pei, Y.; Liu, W.; Crispin, X.; Fabiano, S.; Ma, Y.; et al. Wearable Thermoelectric Materials and Devices for Self-Powered Electronic Systems. *Adv. Mater.* **2021**, *33*, 2102990. [CrossRef] [PubMed]